



# Advanced Dynamic Physical Simulation of Direct Iron Reduction Process in a Steel Plant

By

#### Amin Rooberahan

Presented to the:

Dipartimento Energia (DENERG) of Politecnico di Torino ArcelorMittal Global Research and Development

Under Supervision of:

Prof. Marta Gandiglio (Dipartimento Energia (DENERG))

Prof. Fabio Salomone (Dipartimento Scienza Applicata e Tecnologia (DISAT))

Dr. Antione Moussalem (ArcelorMittal Maizières Research SA)

Maizières-les-Metz, France
August 2025

# Acknowledgements

First of all, I must show my deepest gratitude to my industrial advisor, Antoine Moussalem, whose advice and availability assisted greatly in the development of this project. His technical suggestions and constructive criticism played a determining role in the course and outcome of this work. I am grateful to Raphael Norbert, leader of Energy Team, for his support and insightful opinions that kept enriching my studies throughout. Working for the entire Energy Team has been a delight; their readiness to help and the informal but profoundly professional atmosphere they developed provided a most efficient and pleasant stay at ArcelorMittal. I am equally grateful to Jose Barros Lorenzo, Head of the Process Engineering Department, for his support and for having enabled me to insert my thesis into the wider research activity of the department.

On the academic front, I am thankful to my supervisors from Politecnico di Torino, Prof. Marta Gandiglio and Prof. Fabio Salomone, for the persistent guidance, helpful discussion, and support during the thesis work. I am also thankful to Prof. Fabrice Lemoine and the complete coordination team of the Erasmus Mundus DENSYS program for putting in efforts to arrange and facilitate this distinguished academic experience, which offered me priceless chances throughout Europe.

Finally, I am sincerely grateful to my colleagues, friends, and family, whose encouragement, patience, and support accompanied me through every step of this experience.

#### **Abstract**

The iron and steel industry is one of the largest industrial contributors to global CO<sub>2</sub> emissions, accounting for 7–9% of total anthropogenic emissions. Among available production routes, direct reduced iron (DRI) coupled with an electric arc furnace (EAF) is considered a key pathway for decarbonization, particularly when hydrogen is introduced as a reducing agent. However, the process involves complex thermo-chemical interactions between syngas production, recycling, and multi-zone shaft furnace operation, which remain insufficiently captured in conventional process simulations. This thesis develops, for the first time, a fully integrated dynamic simulation of a MIDREX-type DRI plant. The model was validated against operational data from ArcelorMittal's Contrecœur DRI plant in Canada. For this purpose, an analytical model of the syngas production and shaft furnace cooling process was modeled using AVEVA process engineering software. Then the Analytical model was further developed to an Analytical/Predictive model by adding multiple control loops, which provided more flexibility to the system. The Analytical/Predictive model was coupled through a Python-based bridge code to a 2D MATLAB model of the shaft furnace developed inhouse, enabling iterative data exchange of key flows to establish what is called the Dynamic DRI Virtual Environment (DDRIVE). Furthermore, case studies were conducted to investigate default plant operation and scenarios with additional hydrogen injection into the process gas. The results demonstrate that:

- The deviation between simulation and plant data remained below 5% for all key variables, confirming the robustness of both the analytical and the DDRIVE configurations.
- Default operation reproduced a cold start to steady production of about 63 t/h DRI, from an initial 82 t/h equal to the raw ore feed, with approximately 3 percent deviation relative to plant measurements.
- Hydrogen-injection campaign reproduced seven plant tests at 2600, 3215, 3317, 3412, 3949, 4128, and 4760 Nm<sup>3</sup>/h.
- Specific NG consumption decreased as H<sub>2</sub> injection rose, with a nearly 2 percent drop between 0 and 2600 Nm<sup>3</sup>/h. A reduction of approximately 3.9% is observed at the maximum injection rate of H<sub>2</sub>, 4700 Nm<sup>3</sup>/h.
- Hydrogen addition consistently shifted the process toward a cleaner operating regime, lowering specific CO<sub>2</sub> emissions per tonne of DRI. The 4760 Nm<sup>3</sup>/h injection rate can reduce approximately 3600 tonnes of CO<sub>2</sub> annually.
- Specific Fuel Cost (SFC) analysis showed that while green hydrogen at current prices (C\$7.46/kg) remains prohibitive, blue hydrogen with CCS at C\$2.50–3.10/kg can provide competitive economics up to ~3949 Nm³/h injection rates.

In summary, the developed DDRIVE framework provides a novel and powerful tool for dynamic analysis, offering insights into the operational, energy, and emissions trade-offs associated with hydrogen-based ironmaking.

# **Table of Contents**

Αc	knowle	edgen	nents	11
Ał	stract.			iii
1.	Intro	ducti	on	1
2.	Metl	nodol	ogy	9
	2. 1.	Ana	lytical AVEVA Simulation	9
	2. 1.	1.	Analytical AVEVA Simulation - Configuration	10
	2. 1.	2.	Analytical AVEVA Simulation - Validation	15
	2. 2.	Prec	lictive/Analytical AVEVA Simulation	16
	2. 2.	1.	Predictive/Analytical AVEVA Simulation - Configuration	17
	2. 2.	2.	Predictive/Analytical AVEVA Simulation - Validation	19
	2. 3.	DDI	RIVE – Dynamic DRI Virtual Environment	20
	2. 3.	1.	DDRIVE - Configuration	21
	2. 3.	2.	DDRIVE – Validation	22
3.	Resu	ılts an	nd Case Studies	23
	3. 1.	Defa	ault Plant Operation	24
	3. 2.	H <sub>2</sub> I	njection Case Studies	26
	3. 3.	Futu	re Work	32
4.	Cone	clusio	n	33
5.	Bibl	iograp	phy	35

#### Abbreviation

BF	Blast Furnace	H-DR	Hydrogen Direct Reduction
BOF	Basic Oxygen Furnace	LHV	Lower Heating Value
DDRIVE	Dynamic DRI Virtual Environment	NG	Natural Gas
DRI	Direct Reduced Iron	PFD	Process Flow Diagram
EAF	Electric Arc Furnace	SFC	Specific Fuel Cost

#### Nomenclature

$\mathrm{A}\;(\frac{mol}{g.s.bar^{-41}})$	Arrhenius Constant
$E_a \left( \frac{J}{mol} \right)$	Activation Energy
K index	Equilibrium Constants
k index	Reaction Rate Constant
k Species	Adsorption Constants
r	Rate Equation

#### 1. Introduction

The iron and steel industry is responsible for roughly 7–9% of global CO<sub>2</sub> emissions [1] and approximately 20–25% of CO<sub>2</sub> emissions from industrial processes (approximately 2.6 gigatons of CO<sub>2</sub> annually) [2]. In recent years, global steel production has surged by 16%, rising from 1.62 billion tons in 2015 to 1.89 billion tons in 2023, reflecting the increasing reliance on steel in various industries [3]. This substantial contribution makes it a pivotal target for strategies aimed at meeting the emission reduction targets set by the Paris Agreement, and for mitigating the harmful effects of global climate change [4].

Steel production is currently achieved through three primary methods: the blast furnace paired with the basic oxygen furnace (BF-BOF), the direct reduced iron process combined with an electric arc furnace (DR-EAF), and the electric arc furnace (EAF) approach relying solely on recycled scrap metal. Conventional blast furnace ironmaking operations are characterized by substantial energy consumption and a reliance on high-grade metallurgical coke [5]. About 70% of the world's steel is produced via BF-BOF, which emits an average of 2.3 tons of CO<sub>2</sub> per ton of crude steel [6] which is around ~90% of steel emissions [2]. Currently, the most widely adopted low-CO<sub>2</sub> steel production method relies on recycled scrap. However, this approach is inherently limited by the balance of scrap supply and demand [7]. The direct reduction of iron (DRI) process, when paired with an electric arc furnace (EAF), represents the second most commercialized low-CO<sub>2</sub> steel production method. It offers a viable alternative to scrap-based production, with the flexibility to use iron ore, making it less constrained by scrap availability [8]. Coal-based direct reduced iron (DRI) technology achieves a 38% reduction in CO<sub>2</sub> emissions when compared to the conventional blast furnace-basic oxygen furnace (BF-BOF) ironmaking process, highlighting its potential as a more sustainable alternative. Incorporating methane (CH<sub>4</sub>) alongside hydrogen (H<sub>2</sub>) and carbon monoxide (CO) in DRI production can lower CO<sub>2</sub> emissions by 61% compared to the conventional BF-BOF method. Transitioning entirely to hydrogen-based DRI (H2-DRI) achieves an even greater impact, cutting CO<sub>2</sub> emissions by an impressive 97%, showcasing its potential as a nearly emission-free solution [9].

DRI process uses Hydrogen (H<sub>2</sub>) and carbon monoxide (CO) as highly effective reducing agents. At 900°C, the gas utilization efficiencies for H<sub>2</sub> and CO in the reduction of Fe<sub>2</sub>O<sub>3</sub> are 37.575% and 31.460%, respectively, representing the maximum utilization rates for these gases at this temperature [10]. Syngas production is achieved through two main methods: steam methane reforming, as utilized in the HYL III process, or dry reforming, which is the approach adopted in the Midland-Ross direct reduction (MIDREX) process. The MIDREX (Figure 1) and HYL III processes share similarities but differ in key aspects, particularly in their approach to methane reforming. MIDREX relies on dry methane reforming, whereas HYL III utilizes steam methane reforming, with the added advantage of capturing CO<sub>2</sub> generated during the process. In contrast, MIDREX incorporates CO<sub>2</sub> into the dry reformer, contributing to syngas production. Another major distinction is the operating pressure. MIDREX functions at a lower pressure of roughly 3 bar, while HYL III operates at about 6 bar. The energy consumption for DRI production is comparable between the two methods, with HYL III requiring 10.3 GJ/ton and MIDREX consuming 10.5 GJ/ton. However, HYL III demonstrates greater efficiency in electricity usage, consuming 85 kWh per ton of DRI, while MIDREX requires 130 kWh per ton. In terms of CO<sub>2</sub> emissions, both processes have similar outputs, with HYL III emitting 541 kg/ton of DRI and MIDREX slightly lower at 538 kg/ton [11]. Due to its high implementation rate, representing about 65% of the total worldwide produced DRI [12], the MIDREX process was' selected to be simulated in this study.

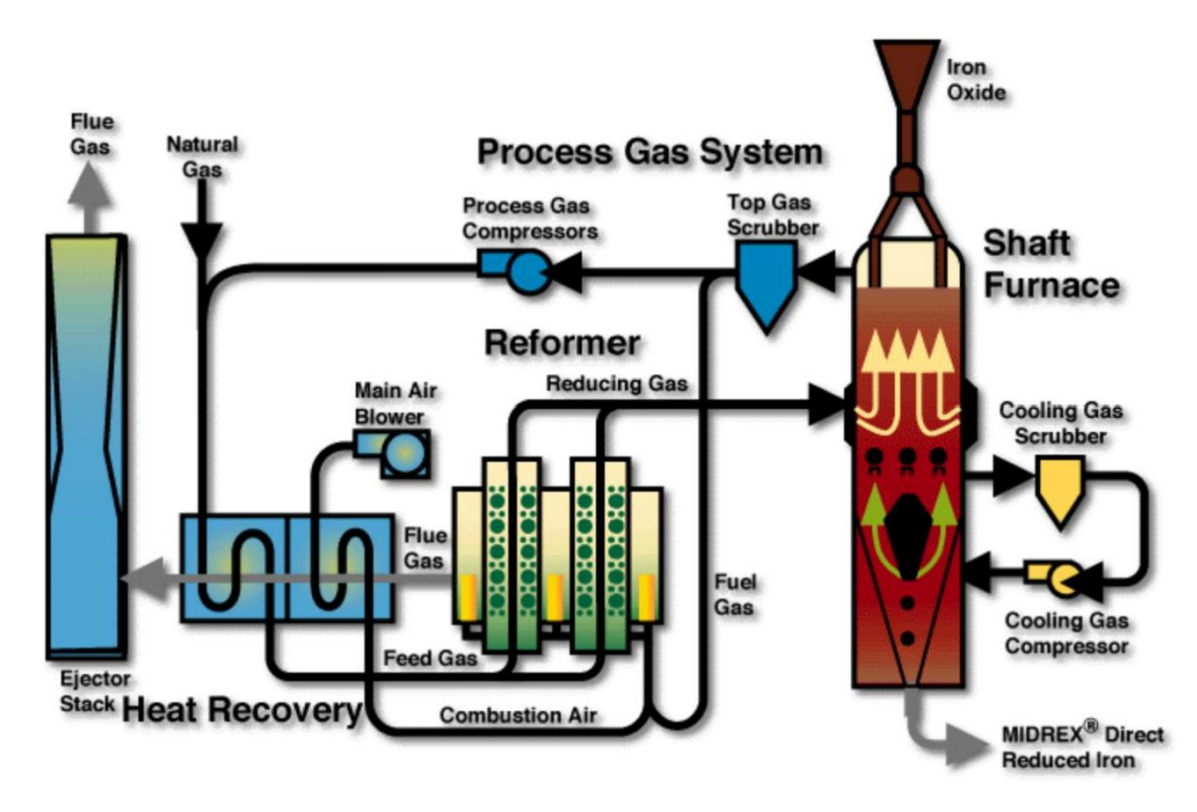


Figure 1. MIDREX direct reduction plant process [13]

The process of directly reducing iron oxide (DRI) involves a complex solid-fluid interaction, characterized by its intricate multi-scale behavior, a system comprising multiple particles, complex reaction kinetics, and a wide range of chemical reactions [14] [15]. The reduction of iron ore proceeds step by step with CO and  $H_2$  through sequential reactions (Fe<sub>2</sub>O<sub>3</sub> $\rightarrow$ Fe<sub>3</sub>O<sub>4</sub> $\rightarrow$ FeO $\rightarrow$ Fe), as presented in Figure 2 [16].

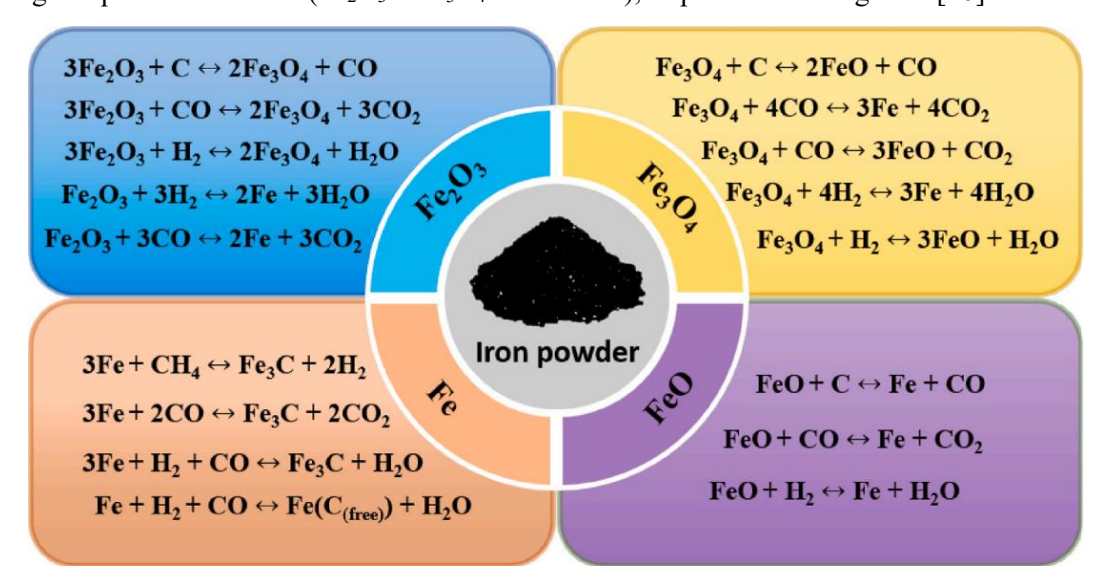


Figure 2. Reaction equations demonstrating DRI production in the shaft furnace

By substituting the H<sub>2</sub>/CO mixture with pure hydrogen as the reducing gas, and producing only water as a byproduct, hydrogen direct reduction (H-DR) emerges as a promising pathway for achieving swift and impactful decarbonization in the steelmaking industry [17] [18]. Although thermodynamically less

favorable due to its endothermic reaction compared to the exothermic behavior of carbon monoxide, hydrogen proves as an efficient reducing gas. Its advantages lie in its higher energy content, lighter density, stronger penetration, and faster reduction kinetics, making it a more efficient and effective choice overall [19]. According to MIDREX, operating entirely with hydrogen would require a total of 900 m³ of H₂ per ton of DRI. Of this amount, 650 m³ would be consumed in the reduction process, while 250 m³ would serve as fuel for the gas heater. Additionally, approximately 50 m³ of natural gas (NG) would be needed to regulate both the temperature and the carbon content of the resulting DRI [20]. Although H₂-DRI offers significant advantages in reducing greenhouse gas emissions compared to CH₄-based DRI, it faces notable challenges. These include higher economic costs, concerns over operational safety, and lower efficiency during high-temperature reduction, making it less competitive in these areas [9]. Moreover, the carbon emission reduction potential of using H₂ as a reducing gas, depends on the source of H₂ production. Currently, Roughly 96% of global hydrogen production relies on fossil fuels, contributing heavily to CO₂ emissions [21].

The growing necessity to reduce CO<sub>2</sub> emissions in the steel industry has driven extensive research efforts focused on simulating direct reduction plants, particularly those utilizing hydrogen as the primary reducing agent. The shaft furnace serves as the core component of the direct reduction process, where iron ore pellets undergo reduction and cooling to produce cold direct reduced iron (DRI). In this system, reducing gas is introduced at an intermediate level of the furnace, flowing upward as it facilitates the reduction of iron ore before being discharged at the top. To cool the reduced iron pellets before they exit the furnace, a cooling gas—typically natural gas—is injected at the bottom. The shaft furnace is a highly complex reactor that consists of distinct zones, thus, to effectively design and optimize it, a thorough understanding of the system's thermodynamics and kinetics is crucial as multiple reactions occur inside the furnace which are summarized in Table 1. A reactor of this complexity cannot be accurately modeled using the standard reactor library available in process simulation software, including AVEVA. Numerous mathematical and numerical models of the shaft furnace were published, differing by the assumptions, the physico-chemical phenomena accounted for, the numerical scheme, the sections of the furnace considered, and the use of the model, etc. The main differences are as follows:

- The number of reduction steps.
- The nature of the inlet gas mixture.
- The number of dimensions included in the geometrical description.
- The description of the pellet transformation: shrinking core or grain models.
- The presence of supplementary reactions.
- The type of heat transfer.
- The presence of the cooling zone.
- Some models were validated against plant data, others not.

Table 1. reactions occur inside the shaft furnace [10]

Reaction Type	Chemical Reaction	Enthalpy (kJ/mol)
	$3Fe_2O_3 + CO = 2Fe_3O_4 + CO_2$	-43.221
	$Fe_3O_4 + CO = 3FeO + CO_2$	19.288
CO Reduction reaction	$FeO + CO = Fe + CO_2$	-10.920
	$Fe_2O_3 + 3CO = 2Fe + 3CO_2$	-23.389
	$3Fe_2O_3 + H_2 = 2Fe_3O_4 + H_2O$	-2.071
	$Fe_3O_4 + H_2 = 3FeO + H_2O$	60.438
H <sub>2</sub> Reduction reaction	$FeO + H_2 = Fe + H_2O$	30.229
	$Fe_2O_3 + 3H_2 = 2Fe + 3H_2O$	100.060
CH <sub>4</sub> reforming reaction	$CH_4 + H_2O = 3H_2 + CO$	206.083
	$CH_4 + CO_2 = 2H_2 + 2CO$	247.233
CH <sub>4</sub> cracking reaction	$CH_4 = C + 2H_2$	74.810
CH <sub>4</sub> reduction reaction	$CH_4 + FeO = Fe + 2H_2 + CO$	236.312
	$Fe_2O_3 + 3CH_4 = 2Fe + 6H_2 + 3CO$	718.309
	$3Fe + 2CO = Fe_3C + CO_2$	-149.829
	$3Fe + CO + H_2 = Fe_3C + H_2O$	-108.679
	$3Fe + CH_4 = Fe_3C + 2H_2$	97.404
Carburizing reaction	$3FeO + 5CO = Fe_3C + 4CO_2$	-182.590
	$3Fe + C = Fe_3C$	22.594
Carbon deposition reaction	$2CO = C + CO_2$	-172.423
Water-gas shift reaction	$CO + H_2O = H_2 + CO_2$	-41.150
Gasification reaction	$C + H_2O = H_2 + CO$	131.273

Ma et al. [22] delineate four interconnected hierarchical levels in the evolution of the reduction process, where changes at the nano- and microstructural scales significantly influence reaction kinetics. These levels include: the atomic scale, focusing on transformations in atomic and molecular structures; the microscale, addressing alterations within the pellet grain structure; the mesoscale, analyzing variations across the pellet radius; and the macroscale, exploring broader changes occurring throughout the reactor system [23]. At the pellet scale, numerous studies have emphasized notable differences in the reduction behavior of iron ore when using pure hydrogen compared to the conventional H<sub>2</sub>-CO gas mixture. These distinctions arise from variations in reaction kinetics, gas-solid interactions, and byproduct formation, which play a critical role in determining the efficiency and sustainability of the reduction process. Firstly, the reduction rate using pure hydrogen is substantially higher compared to that with pure CO. This leads to an enhanced reaction rate as the H<sub>2</sub>:CO ratio increases, showcasing the efficiency of hydrogen in the reduction process [24] [25] [26] [27]. From a thermodynamic standpoint, the solid-phase transitions of hematite, magnetite, wustite, and iron exhibit distinct behaviors under varying temperatures, depending on whether hydrogen or a hydrogencarbon monoxide mixture is used as the reducing gas. These differences arise from the unique reaction pathways and energy requirements associated with each gas [28]. Moreover, carbon deposition caused by the Boudouard reaction is a significant issue in processes utilizing CO, as it drastically reduces the reduction rate. This challenge, however, is entirely avoided when pure hydrogen is employed as the reducing gas [27]. At a reduction temperature of 900°C, the process involving CO as a reducing gas has been reported to cause noticeable swelling of the pellet, leading to an increase in its overall volume [23] [29]. In contrast, when hydrogen is employed, the volume change has been minimal or nearly negligible, underscoring the advantages of hydrogen-based reduction [30]. Metolina et al. [31] employed a 2D axisymmetric finite

element model of pellet grains to examine how temperature influences the morphological transformations in industrial pellets during isothermal reduction. Simulations highlighted the shift in controlling mechanisms from chemical kinetics at lower temperatures (600–700 °C) to mixed diffusion-kinetic control at higher temperatures (800–900 °C). The study further revealed that porosity increased from 34% to 59% during reduction, affecting gas diffusion and pellet performance.

Moving further to simulating the complete DRI plant, Müller et al. [32] evaluated the impact of DRI on the blast furnace process by modeling a blast furnace based on literature data and implemented in Aspen Plus. Additionally, a detailed simulation of a state-of-the-art direct reduction plant (DRP) was conducted to assess the feasibility of replacing natural gas with hydrogen as the reducing agent. Two variations of the HYL III in-situ reforming process were examined—one utilizing a gas-based preheater and the other incorporating an electrical preheater, as illustrated in Figure 3. The shaft reactor was modeled as two counter-currently operating RIGBBS reactors to replicate the behavior of a moving bed reactor. These modeled process steps were integrated to form a complete hot metal production route. By adjusting the boundary conditions of the DRP and tracking the CO<sub>2</sub> emissions from both process steps, the overall potential for emission reduction was evaluated. The simulation results indicated that, under optimal conditions, CO<sub>2</sub> emissions could be reduced by up to 25.8% compared to conventional blast furnace operations. However, partial substitution of natural gas with hydrogen alone does not guarantee significant CO<sub>2</sub> reduction unless renewable energy is used for electrolysis. Likewise, the use of an electrical preheater can contribute to lower emissions, but its effectiveness depends on sourcing power from renewable energy rather than gas-based heating.

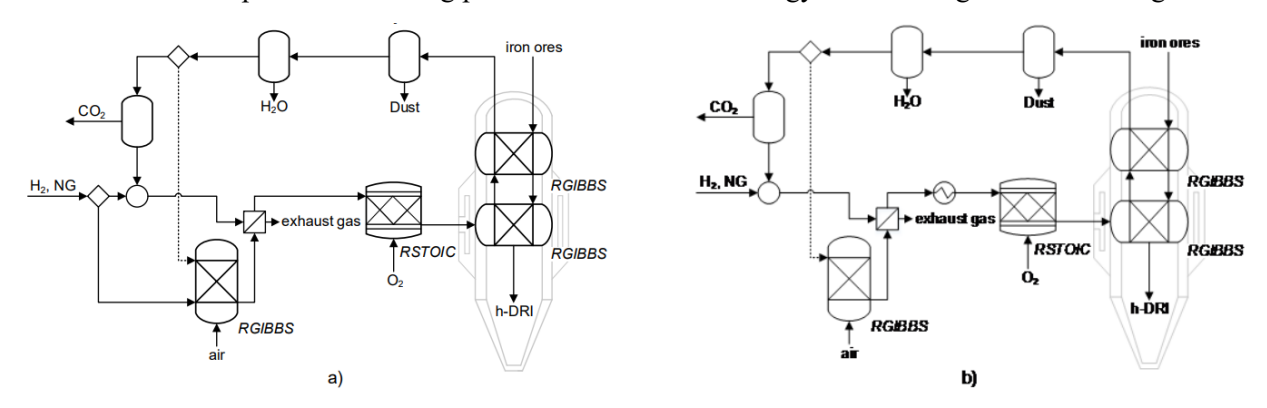


Figure 3. Simplified flowsheet of the DRP model with a) gas-heated and b) electrically heated reducing gases of Müller et al. [32].

Béchara et al. [33] conducted a simulation of a MIDREX-based direct reduction plant with the objective of optimizing process parameters to achieve lower CO<sub>2</sub> emissions, utilizing ASPEN PLUS for the analysis, as illustrated in Figure 4. The shaft furnace was modeled through a customized approach, derived from a 2D mathematical model implemented in FORTRAN which was validated against data of the ArcelorMittal Contrecœur plant, Canada. Their findings demonstrated that by optimizing operational parameters alone—without altering the fundamental process—it was possible to achieve a 15% reduction in CO<sub>2</sub> emissions.

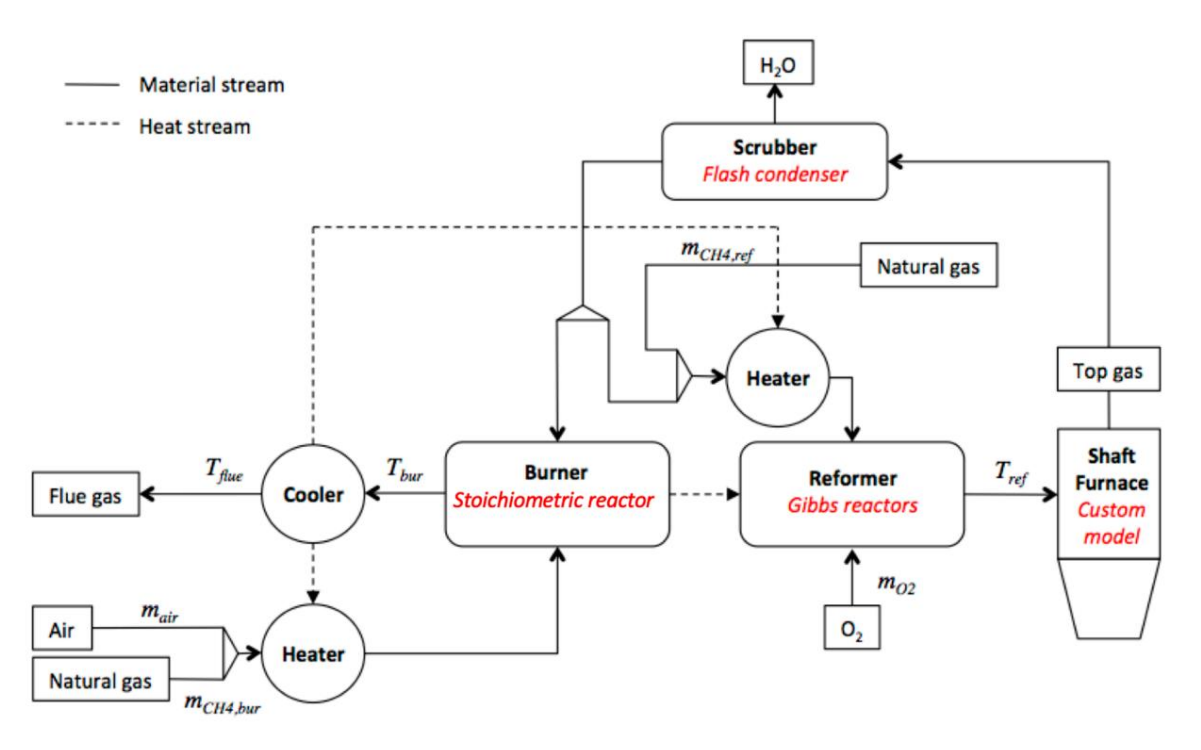


Figure 4. Modeled MIDREX process flow diagram, with its gas loop by Béchara et al. [33].

Rechberger et al. [34] simulated a MIDREX-based hydrogen direct reduction plant using m.SIMTOP, analyzing two alternative cases in addition to a reference scenario. The first approach explored the gradual replacement of natural gas with hydrogen for iron ore reduction, while the second focused on a hydrogen-driven reduction process with a controlled natural gas input of 48 m³ stp per ton of DRI to regulate carbon content, as shown in Figure 5 – a. Their findings reveal a substantial decrease in CO<sub>2</sub> emissions, dropping from about 450 kg per ton of DRI to nearly 50 kg per ton as the ratio of hydrogen to total process gas increases from zero to one. Moreover, the study emphasizes the critical role of hydrogen production methods, particularly electrolysis, in determining the overall carbon footprint of the process. The authors identified a threshold value of approximately 120 g CO<sub>2</sub> per kWh for electricity-related emissions, beyond which hydrogen-based direct reduction becomes less advantageous.

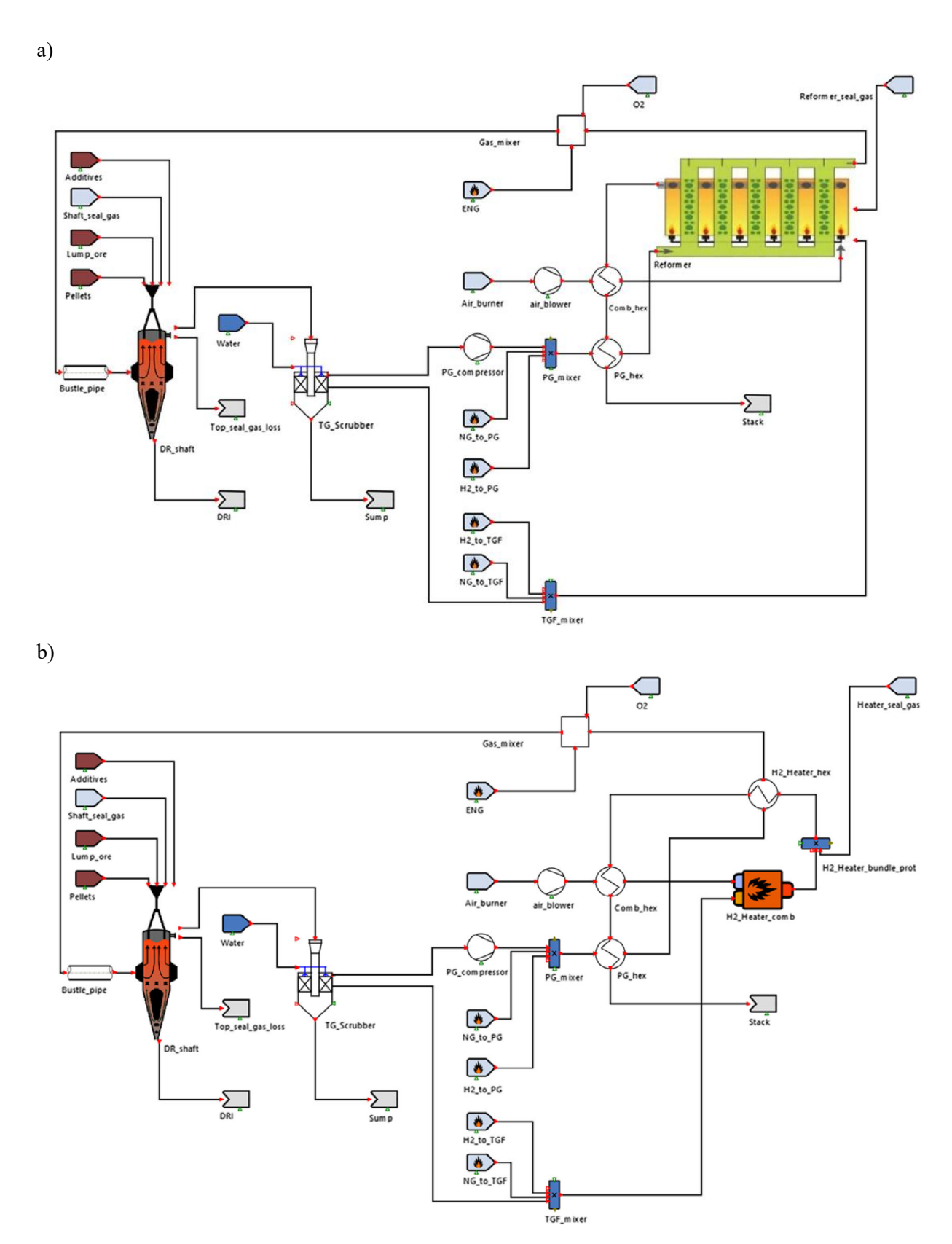


Figure 5. (a) Process model for (NG-based) DR-NG process with addition of hydrogen (b) Process model for (hydrogen-based) DR-H2 process [34].

7 - Advanced Dynamic Physical Simulation of Direct Iron Reduction Process in a Steel Plant

Immonen and Powell [35] developed a physics-based dynamic 1-D model of for the reduction section of a DRI shaft furnace through transient case studies with different compositions of the syngas. The model's accuracy has been validated using industrial data, achieving mean average errors of 0.3 wt% for the outlet solids composition and 1.2 mol% for the outlet gas composition. The model is capable of simulating four-hour transient tests in less than three minutes on a standard computer.

Alsaedi [36] used ASPEN PLUS V12 to simulate HYL III/MIDREX and hydrogen-based shaft furnaces across five direct reduction plant configurations. A techno-economic analysis for the UAE indicated that the Modified HYL III could cut emissions by 24% while remaining cost-effective. In contrast, although Modified MIDREX achieved a 35% reduction in CO<sub>2</sub> emissions, its high operational costs outweighed the benefits, making it unfeasible for decarbonization.

While several studies have modeled the DRI plant, the literature lacks a fully dynamic simulation that couples detailed syngas production with an advanced shaft furnace model. This thesis addresses that gap by developing, for the first time, an integrated, dynamic, and physically detailed simulation of the entire DRI process. To achieve this, the plant is conceptually divided into two main sections (Figure 6). The first section includes the syngas production process and cooling zone, which are modeled using 0D and 1D elements in AVEVA Process Simulation. This allows for precise characterization of flow properties across key process units. The second section focuses on the shaft furnace, the core of the DRI process. A two-dimensional (2D) furnace model, developed in-house at ArcelorMittal using MATLAB, is employed to capture the spatial dynamics and reaction kinetics within the reactor. To couple these two modeling environments, a custom Python-based bridge is developed, enabling real-time data exchange between AVEVA and MATLAB. This iterative coupling results in a robust, dynamically consistent simulation of the full DRI process. The dynamic simulation is validated against real Contrecoeur, Canada ArcelorMittal plant data.

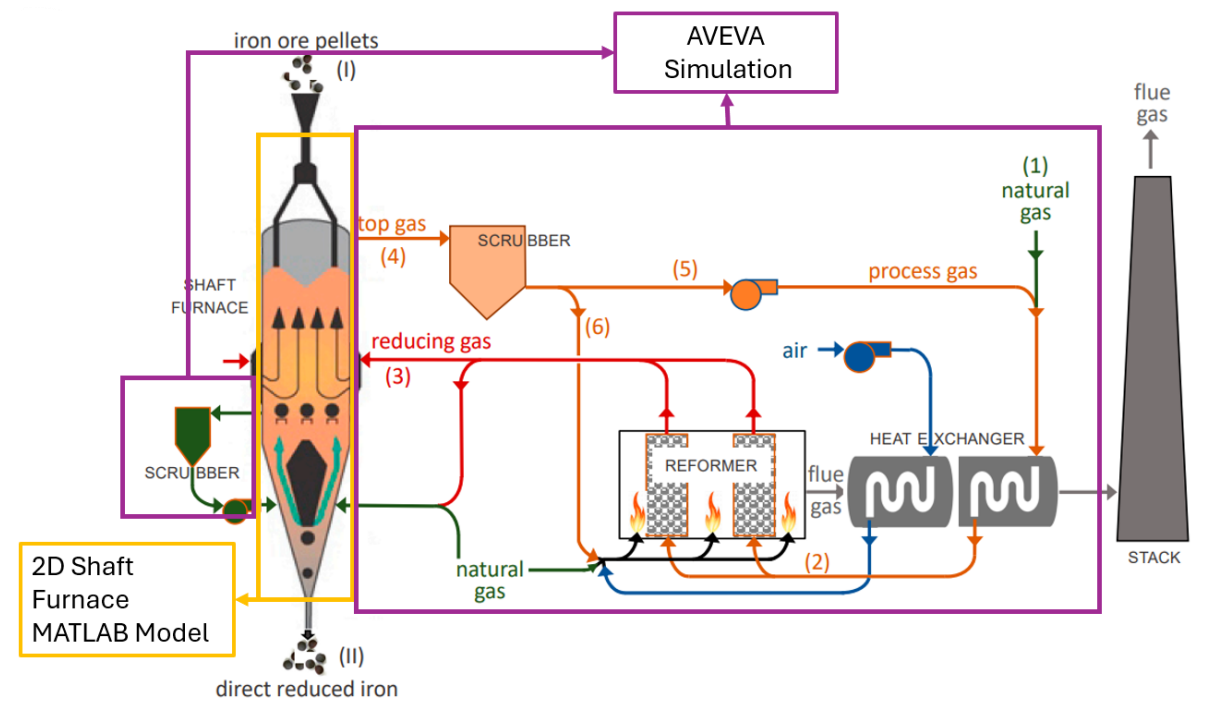


Figure 6. Division of the MIDREX-type direct reduction process into two general parts for achieving a robust dynamic simulation

# 2. Methodology

In this thesis, a comprehensive model of Contrecoeur, Canada ArcelorMittal DRI plant with the auxiliaries is simulated. The Process Flow Diagram (PFD) of the plant is shown in **Error! Reference source not found.** For the purpose of simulating the reducing gas production and cooling zone of DRI plant, AVEVA Process Simulation (called AVEVA now on) was used.

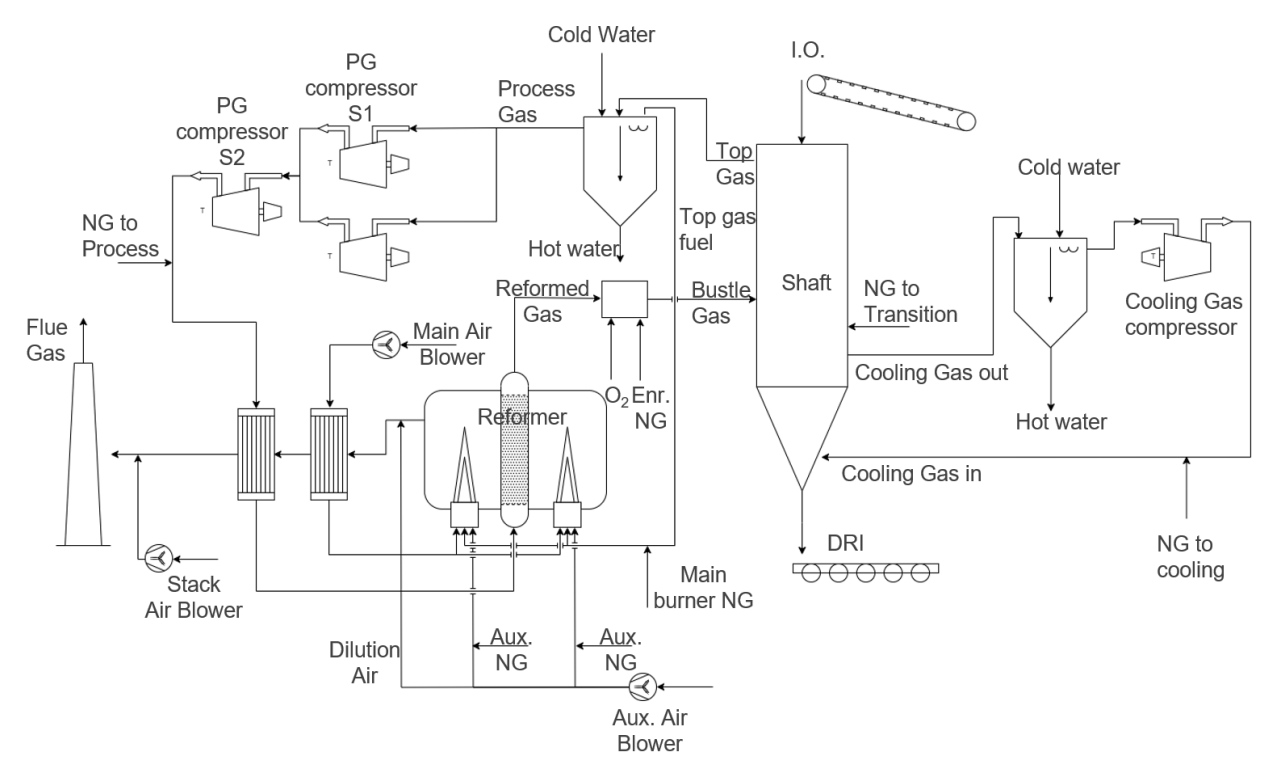


Figure 7. DRI Plant PFD

To achieve a full dynamic simulation process of the plant, models at different levels were developed. First, a model replicating a specific state of the plant using 0D or 1D modelling of the process steps, called "Analytical AVEVA Simulation", is developed. Then, this model is enhanced to the "Predictive/Analytical AVEVA Simulation" by applying some control loops to give more degree of freedom and thus predictive capabilities to the simulation. In the next step, the "Predictive/Analytical AVEVA Simulation" simulation is connected to an advanced 2D MATLAB model of the shaft furnace, developed in house in ArcelorMittal, through a bridge code developed in Python. The full connection of 2D MATLAB Shaft furnace model to "Predictive/Analytical AVEVA Simulation" makes the "Dynamic DRI Virtual Environment (DDRIVE)" that can simulate continuous production of a MIDREX DRI plant. All the simulations above are compared and validated against real plant data.

In the next parts of this chapter the methodology of developing each step of simulations mentioned above and its validation is presented.

# 2. 1. Analytical AVEVA Simulation

As mentioned before, a process simulation of Contrecoeur, Canada ArcelorMittal DRI plant capable of resembling specific plant operation state is modeled in AVEVA as the first step. In this section, a more

9 - Advanced Dynamic Physical Simulation of Direct Iron Reduction Process in a Steel Plant

detailed explanation of each part of the simulation which is called "Analytical AVEVA Simulation" is given.

# 2.1.1. Analytical AVEVA Simulation - Configuration

In the first stage of a DRI plant, top gas is extracted from the shaft furnace at high temperature and contains various impurities, including fine particulate matter, unconverted hydrocarbons, and condensable species. To condition this gas for reuse, it is directed to a top gas scrubber where it is cooled and cleaned through direct contact with injected cold water. This top gas scrubber is modeled as a 1D scrubber with the real dimensions the scrubber in the plant. Afterwards, a part of the cool top gas is sent to the burner to be used as fuel for the burner and the rest is recycled as process gas. This part of simulation is shown in Figure 8.

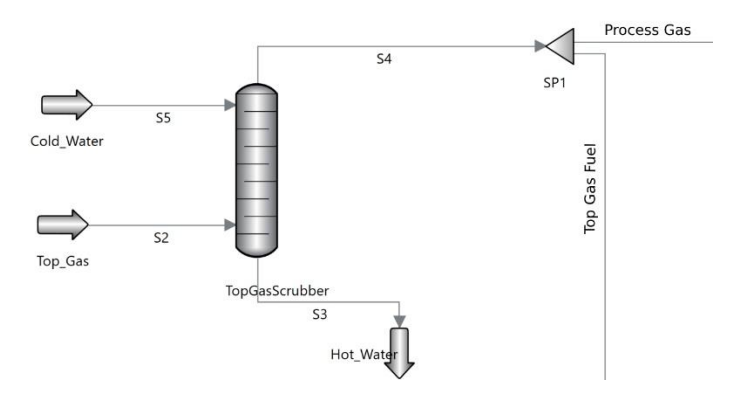


Figure 8. Top Gas Scrubber

After cooling and purifying the top gas in the top gas scrubber, the process gas goes through a two-step compression stage as shown in Figure 9. The lube compressors are used in the DRI plant. Thus, before each compressor a humidifier is applied. A recycle stream is incorporated downstream of the final compression stage to maintain minimum flow requirements, prevent surge conditions, and support process stability. A This part is simulated as a 0D model with compressors operating at constant power. Following the mixing of recycled process gas and cold natural gas, the mixture is directed to a knockout drum (V4). This vessel allows for the removal of any condensed water or entrained liquids that may form due to the temperature drop or pressure changes during mixing ensuring that only clean, dry gas proceeds downstream for reforming.

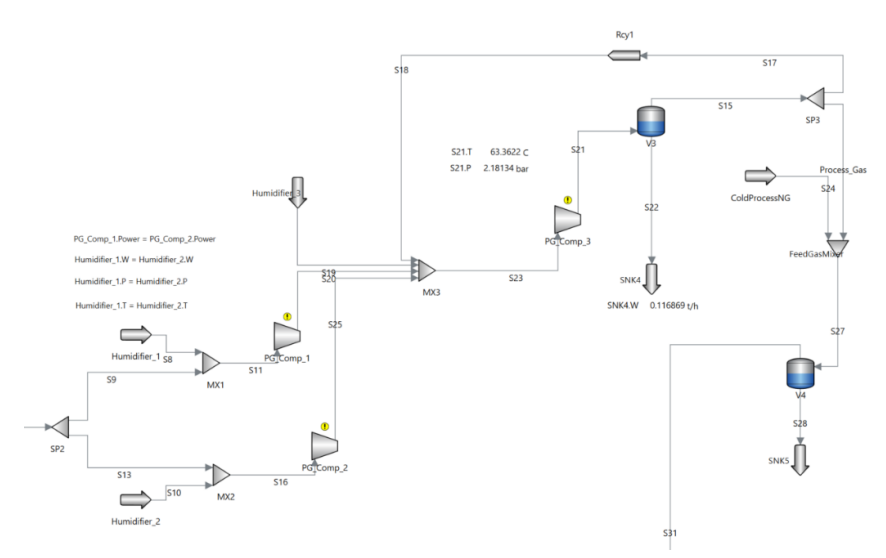


Figure 9. Two stage compression

10 - Advanced Dynamic Physical Simulation of Direct Iron Reduction Process in a Steel Plant

As seen in Figure 10, 0D model of the main burner of the plant is fed by the cold fuel gas coming from the top gas scrubber, the main NG and the auxiliary NG and air. The flue gas of the burner is used for two preheating stages. First, preheating the main air of the burner and then for preheating the cold feed gas. All heat exchangers are modeled with 1D method including the dimensions of the counter flow tubes. The heat produced in the burner is fed to the reformer using an on-canvas equation (1.14 \* E1.Duty = Reformer.Duty). 14% of extra heat being allocated to the reformer is to count for the heat losses in the burner and reformer not being considered in the simulation. Combustion reactions accruing in the burner are:

$$CH_4 + 2O_2 \leftrightarrow CO_2 + 2H_2O \tag{1}$$

$$C_2H_6 + 3.5O_2 \leftrightarrow 2CO_2 + 3H_2O \tag{2}$$

$$C_3H_8 + 5O_2 \leftrightarrow 3CO_2 + 4H_2O$$
 (3)

$$C_4 H_{10} + 6.5 O_2 \leftrightarrow 4C O_2 + 5 H_2 O \tag{4}$$

$$H_2 + 0.5O_2 \leftrightarrow H_2O \tag{5}$$

$$CO + 0.5O_2 \leftrightarrow CO_2 \tag{6}$$

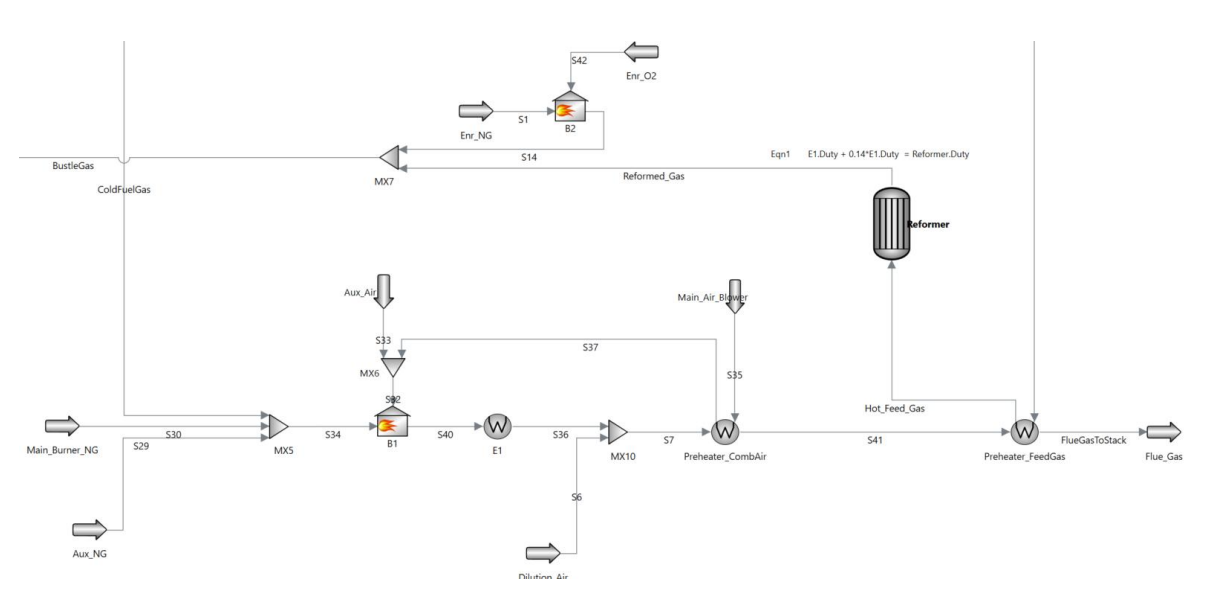


Figure 10. Burner, pre-heaters and reformer

In DRI production, process gas reforming is a critical process that generates the reducing gases (CO and H<sub>2</sub>) necessary for iron ore reduction. This process is modeled using a 1D method of reformer modeling considering the length, diameter and number of the tubes. A kinetic model based on the Langmuir–Hinshelwood mechanism, originally developed by Xu and Froment [37], is employed to describe the steam methane reforming process over a Ni / MgAl<sub>2</sub>O<sub>4</sub> catalyst. This model accounts for both the endothermic reforming reactions (Eqs. (7) and (8)) and the exothermic water-gas shift reaction (Eq. (9)).

Reforming Reaction 1: 
$$CH_4 + H_2O \leftrightarrow CO + 3H_2$$
 (7)

Reforming Reaction 2: 
$$CO + H_2O \leftrightarrow CO_2 + H_2$$
 (8)

Reforming Reaction 3: 
$$CH_4 + 2H_2O \leftrightarrow CO_2 + 4H_2$$
 (9)

The kinetics of the dry reforming reaction:

$$CH_4 + CO_2 \leftrightarrow 2CO + 2H_2 \tag{10}$$

are negligible with respect to the steam reforming reactions (reactions (7) and (9)) [38]. The authors reached the following rate equations:

$$r_1 = k_1 \left( \frac{P_{CH_4} P_{H_2O}}{P_{H_2}^{2.5}} - \frac{P_{H_2}^{0.5} P_{CO}}{K_1} \right) / DEN^2$$
(11)

$$r_2 = k_2 \left( \frac{P_{CO} P_{H_2O}}{P_{H_2}} - \frac{P_{CO}}{K_2} \right) / DEN^2$$
 (12)

$$r_3 = k_3 \left( \frac{P_{CH_4} P_{H_2O}}{P_{H_2}^{3.5}} - \frac{P_{H_2}^{0.5} P_{CO_2}}{K_1 K_2} \right) / DEN^2$$
 (13)

With:

$$DEN = 1 + k_{CO}P_{CO} + k_{H_2}P_{H_2} + k_{CH_4}P_{CH_4} + \frac{k_{H_2O}P_{H_2O}}{P_{H_2}}$$
(14)

In this context,  $P_i$  represents the partial pressure of species *i*. The formulations for the reaction rate constants  $k_1$ ,  $k_2$ , and  $k_3$ , as well as the adsorption constants for CO,  $H_2O$ ,  $CH_4$ , and  $H_2$ , are outlined in Table 2, along with the equilibrium constants  $K_1$  and  $K_2$ .

Table 2. Reaction rate constants, absorption constants and the equilibrium constants of reformer

Parameters	Value
$k_1$	$9.49 \times 10^{15} \exp{(\frac{-240.1}{RT})}$
$k_2$	$4.39 \times 10^6 \exp{(\frac{-67.13}{RT})}$
$k_3$	$2.29 \times 10^{15} \exp{(\frac{-243.9}{RT})}$
$k_{CO}$	$8.23 \times 10^{-5} \exp\left(\frac{-70.65}{RT}\right)$
$k_{CH_4}$	$6.65 \times 10^{-4} \exp\left(\frac{-38.28}{RT}\right)$
$k_{H_2O}$	$1.77 \times 10^5 \exp{(\frac{-88.68}{RT})}$

$k_{H_2}$	$6.12 \times 10^{-9} \exp{(\frac{82.9}{RT})}$
$K_1$	$\exp\left(\frac{-26830.0}{T} + 30.114\right)$
$K_2$	$\exp\left(\frac{4400}{T} - 4.036\right)$
$K_3$	$K_1 * K_2$

The corresponding reaction rate expressions describing CO and CO<sub>2</sub> formation, along with methane consumption during steam reforming, are derived as follows:

$$r_{CO} = r_1 - r_2 \tag{15}$$

$$r_{CO_2} = r_2 + r_3 \tag{16}$$

$$r_{CH_4} = r_1 + r_3 \tag{17}$$

Given the presence of minor concentrations of  $C_2H_6$  (0.32%) and  $C_3H_8$  (0.01%) in the Hot Feed Gas and their complete conversion during the reforming process, the corresponding reforming reactions have been incorporated into the model formulation:

Reforming Reaction 4: 
$$C_2H_6 + 2H_2O \leftrightarrow 2CO + 5H_2$$
 (18)

Reforming Reaction 5: 
$$C_3H_8 + 3H_2O \leftrightarrow 3CO + 7H_2$$
 (19)

Reaction rate for ethane reforming is:

$$r_4 = \frac{k_4}{P_{H_2}^{2.5}} \left( P_{C_2 H_6} P_{H_2 O}^2 - \frac{P_{H_2}^5 P_{CO}^2}{K_1} \right) / DEN^2$$
 (20)

Rate constant equation is given by Arrhenius equation:

$$k = A. \exp\left(\frac{-E_a}{R.T}\right) \tag{21}$$

In which A  $(\frac{mol}{g.s.bar^{-41}})$  is the Arrhenius Constant and  $E_a$   $(\frac{J}{mol})$  is the activation energy which are 46.4  $\frac{mol}{g.s.bar^{-41}}$  [39] and 79.1  $\frac{kJ}{mol}$  [40], respectively. Thus:

$$k_4 = 46.4 \exp\left(\frac{-79100}{R.T}\right) \tag{22}$$

and adsorption constants [41] (wrong):

$$k_{C_2H_6} = 3.275 \times 10^{-6} \exp\left(\frac{-82000}{RT}\right)$$
 (23)

13 - Advanced Dynamic Physical Simulation of Direct Iron Reduction Process in a Steel Plant

Equilibrium constant:

$$K_4 = \exp\left(\frac{-41777.48}{T} + 53.108\right)$$
 (24)

After reforming, the process stream undergoes a combustion enrichment step, where enrichment NG and oxygen are partially combusted in burner B2. The resulting hot combustion gases are mixed with the reformed gas to produce the final bustle gas, which is used downstream in the shaft furnace. The partial combustion reactions accruing in the burner alongside the complete combustion are:

$$CH_4 + 1.5O_2 \leftrightarrow CO + 2H_2O$$
 (25)

$$C_2H_6 + 2.5O_2 \leftrightarrow 2CO + 3H_2O \tag{26}$$

$$C_3H_8 + 3.5O_2 \leftrightarrow 3CO + 4H_2O \tag{27}$$

$$C_4H_{10} + 4.5O_2 \leftrightarrow 4CO + 5H_2O$$
 (28)

On the other side of the shaft furnace, cooling loop (Figure 11) serves to regulate the temperature of the shaft furnace's peripheral zones by circulating conditioned gas through a controlled cooling and recirculation system. This not only protects the refractory and metallic structures from thermal stress but also enhances process stability and ensures consistent reduction conditions throughout the operation.

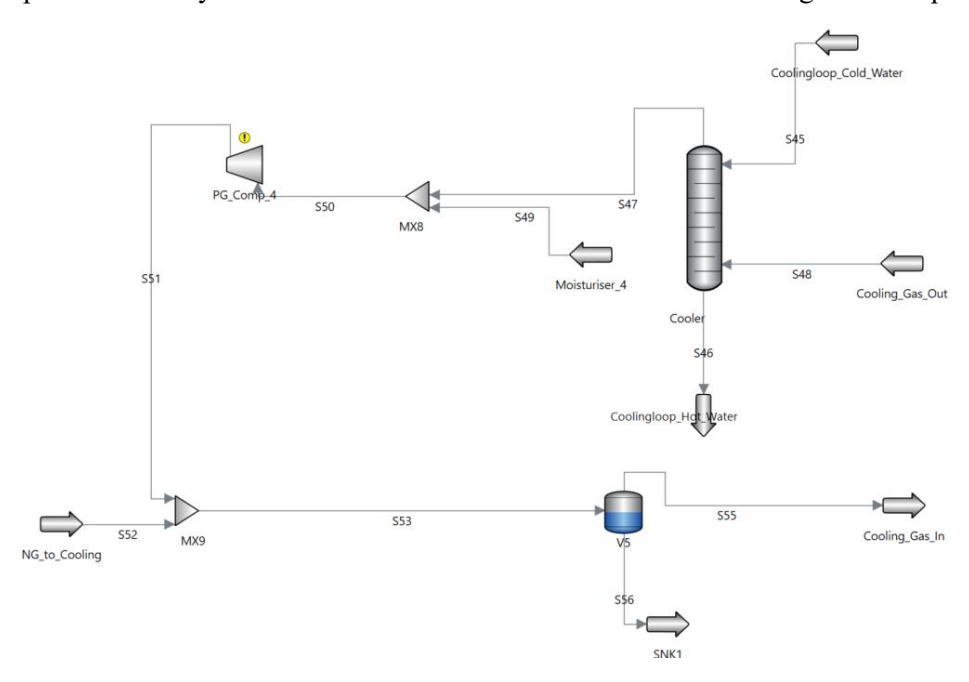


Figure 11. Cooling loop of the DRI plant

The cooling loop is consisting of a 1D model of the scrubber to cool and purify the cooling gases coming from the shaft. Then the gasses go through a compression stage and then NG is injected to ensure a constant flow rate of Cooling Gas In for the shaft.

#### 2. 1. 2. Analytical AVEVA Simulation - Validation

After designing the plant in AVEVA Process Simulation, the results of the simulation were validated against the plant data. Three key parameters—temperature, flow rate, and average gas composition—were selected for this comparison, as they are measured and reported within the operational plant and their deviation is presented in Figure 12. The deviation between the simulated and measured values was calculated using the following formula:

$$Deviation (\%) = \left| \frac{Plant \ data - Simulation \ data}{Plant \ data} \right| \times 100$$
 (29)

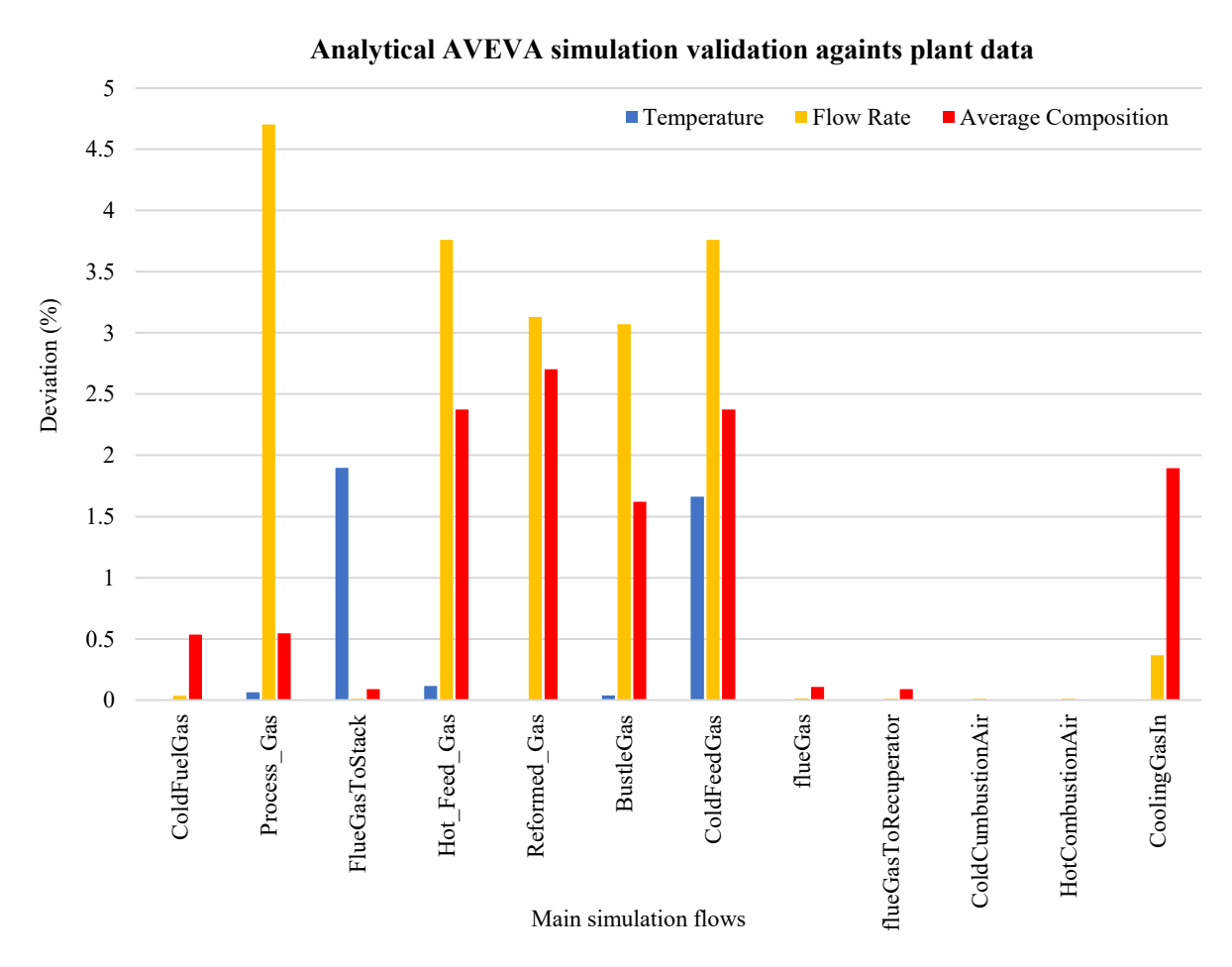
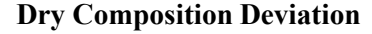


Figure 12. Deviation percentage of Analytical AVEVA simulation validation against plant data

As illustrated, the deviation remains below 5% for all major flow streams across the three evaluated parameters. This low deviation confirms the reliability and accuracy of the analytical simulation in replicating real plant behavior and provides a strong foundation for the subsequent predictive modeling phases.

In addition to the validation of overall process parameters, the dry gas compositions of three key flows, Process Gas, Reformed Gas, and Bustle Gas, were also assessed to verify the accuracy of the analytical simulation. The deviations between simulated and measured molar fractions of the major components (CO<sub>2</sub>, CO, H<sub>2</sub>, CH<sub>4</sub>, and N<sub>2</sub>) are presented in Figure 13:



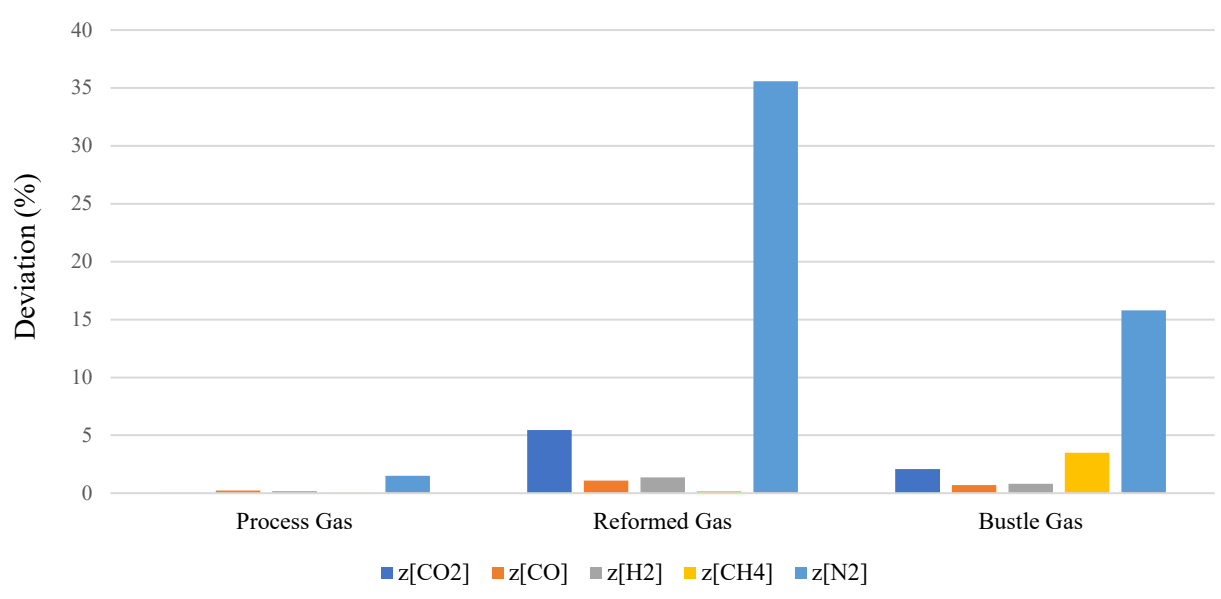


Figure 13. Dry composition percentage error of simulation

As shown, all chemical species exhibit deviations below 5%, except for nitrogen  $(N_2)$  mole fraction in the Reformed Gas and Bustle Gas streams, which show relatively high percentage deviations of 35.64% and 15.80%, respectively. However, this apparent discrepancy stems from the small magnitude of  $N_2$  in the dry gas composition. As presented in Table 3, the absolute deviation in  $N_2$  content is only 0.53% for the Reformed Gas and 0.26% for the Bustle Gas.

Table 3. N2 percentage in the dry composition of simulation and plant measurements

#### N2 in the dry composition (%)

	<u> </u>	
Stage	Reformed Gas	Bustle Gas
Plant data	1.49	1.70
Simulation data	2.02	1.96
Absolute Deviation (%)	0.53	0.26

Nevertheless, the origin of this deviation was further investigated. Since nitrogen is an inert species and does not participate in either reforming or combustion reactions, the discrepancy is unlikely to result from modeling errors. Instead, a review of plant data revealed a mass imbalance in nitrogen flows, suggesting potential sensor miscalibration or measurement error in the plant analyzers. Given the small absolute deviation and confirmed inconsistency in the reference data, the simulation results were deemed acceptable, and the model development proceeded to the next phase.

# 2. 2. Predictive/Analytical AVEVA Simulation

Building upon the validated analytical AVEVA model, which was developed to replicate a fixed plant operation, the simulation was further extended to incorporate predictive capabilities. This enhancement aimed to increase the model's flexibility by allowing the simulation of various operating scenarios. To enable this, several key parameters were unspecified and replaced with control loops featuring adjustable

16 - Advanced Dynamic Physical Simulation of Direct Iron Reduction Process in a Steel Plant

setpoints. This configuration allows the model to dynamically respond to different boundary conditions and process targets.

The following section outlines the implementation of these control loops and presents the corresponding validation of the enhanced predictive simulation.

#### 2. 2. 1. Predictive/Analytical AVEVA Simulation - Configuration

The first control loop was introduced to regulate the pressure of the process gas downstream of the compression stage. This is achieved by adjusting the return flow rate through a feedback loop, ensuring the desired outlet pressure is maintained. The schematic and control settings are presented in Figure 14.

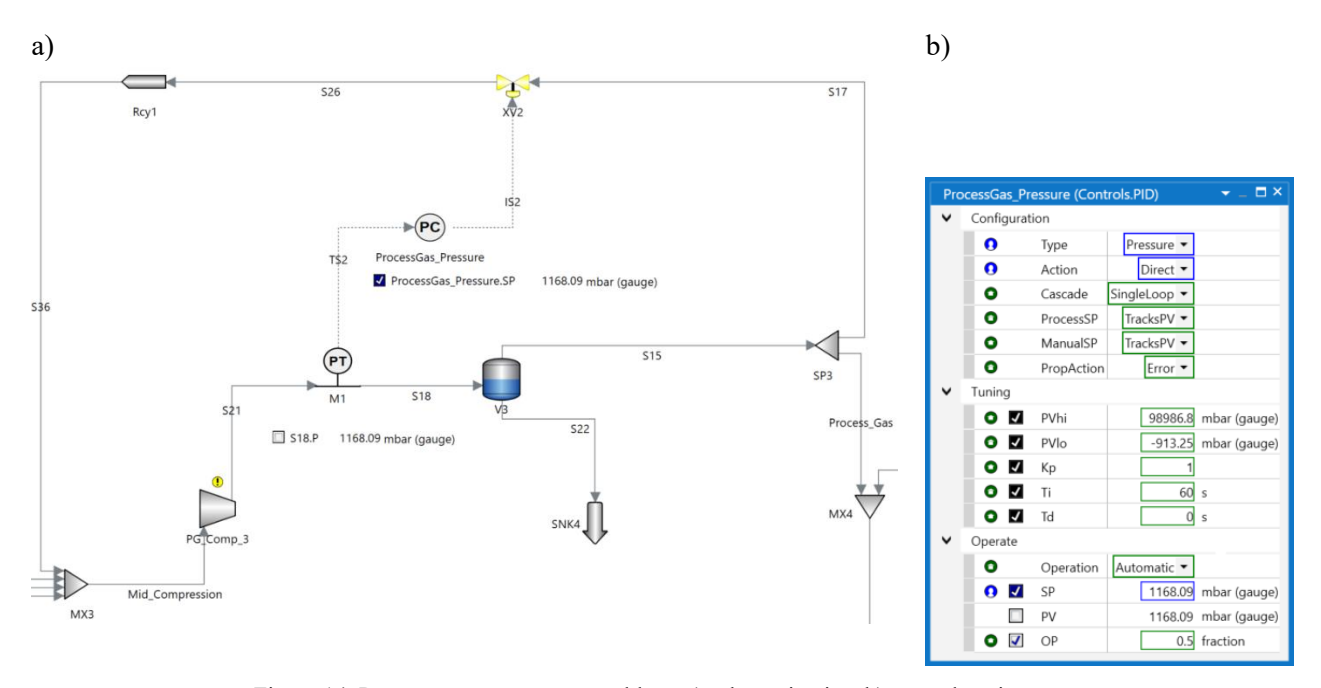


Figure 14. Process gas pressure control loop a) schematic view b) control setting

To maintain a specific CH<sub>4</sub> mole fraction in the Reformed Gas, a control loop was implemented. This loop dynamically modifies the flow rate of Cold Process NG. The setup of this control loop is illustrated in Figure 15.

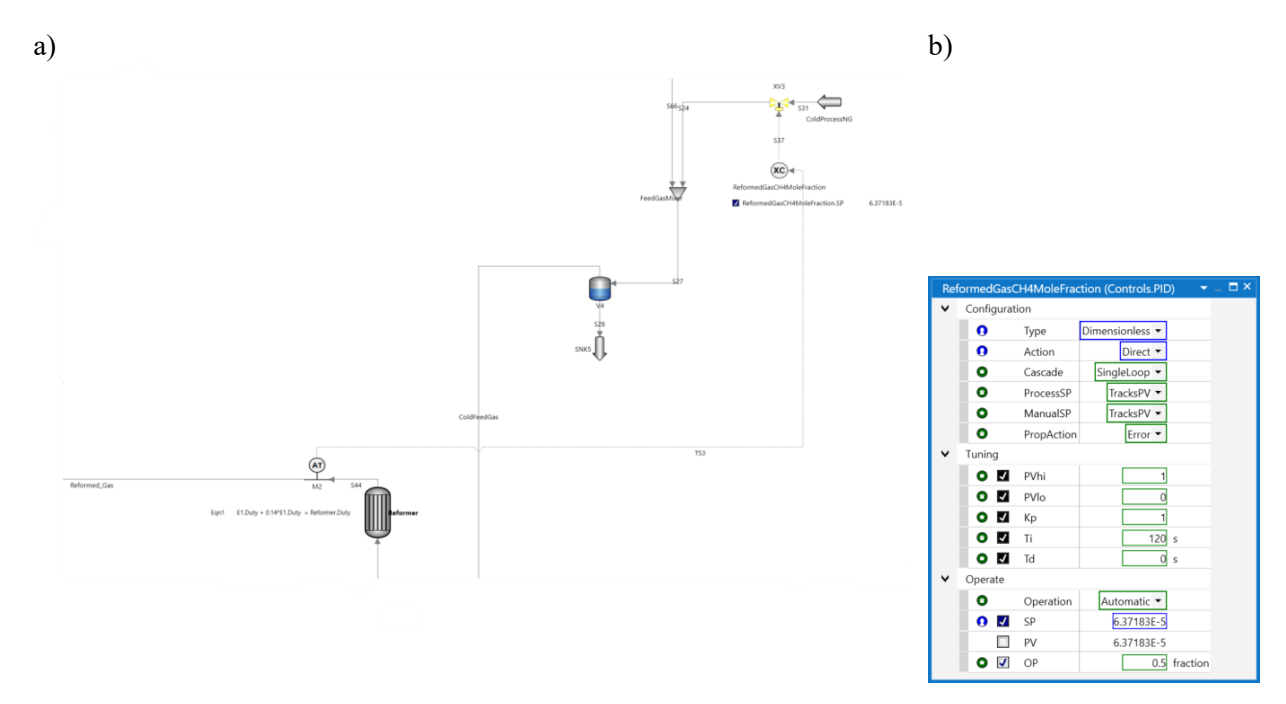


Figure 15. Reformed gas CH<sub>4</sub> mole fraction control loop a) schematic b) setting

Two additional control loops were applied to regulate temperature conditions in the burner and recuperator sections. The first adjusts the Main Burner NG flow rate to maintain the Flue Gas temperature at the burner outlet. The second loop controls the Flue Gas to Recuperator temperature by varying the dilution air flow rate. These mechanisms ensure thermal stability and are presented in Figure 16.

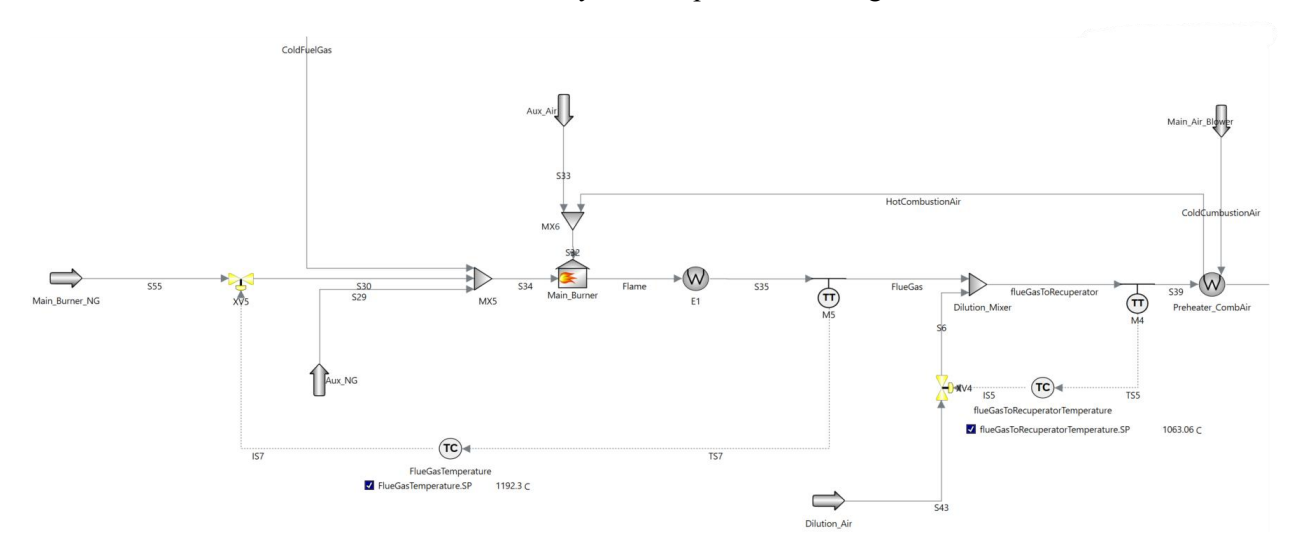


Figure 16. Flue gas and flue gas recuperator temperature control loops

To control both the CH<sub>4</sub> mole fraction and temperature of the bustle gas, two separate control loops were introduced. The CH<sub>4</sub> content is regulated through the enrichment NG flow rate, while the temperature is managed via the oxygen flow rate. The setup of these control loops is depicted in Figure 17.

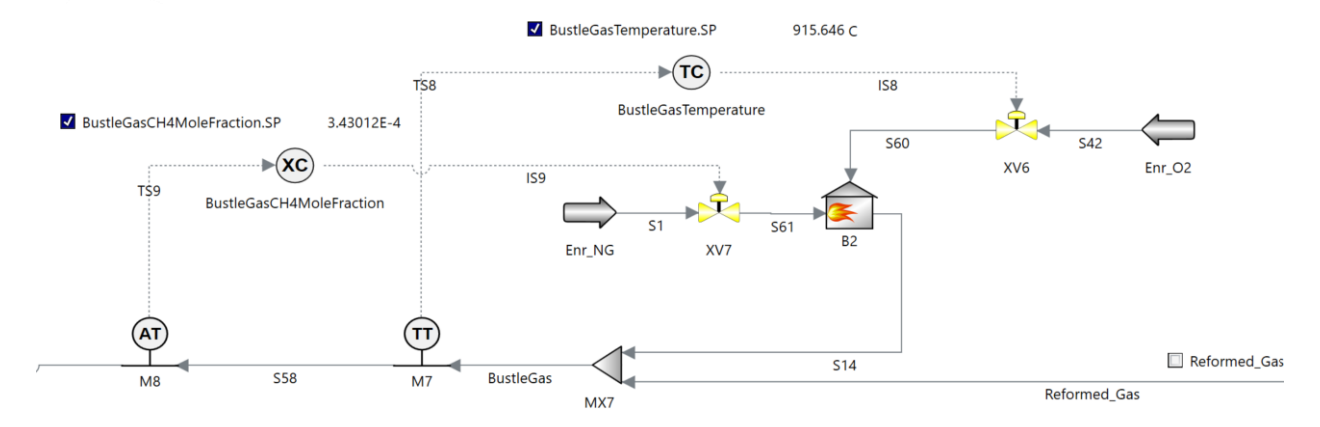


Figure 17. Bustle gas CH<sub>4</sub> mole fraction and temperature control loops

A final control loop was implemented in the cooling zone to maintain a constant Cooling Gas In flow rate. This is accomplished by automatically adjusting the NG to Cooling flow rate. The configuration is presented in Figure 18.



Figure 18. Cooling Gas In flow rate control loop

# 2. 2. 2. Predictive/Analytical AVEVA Simulation - Validation

To verify the correct implementation and performance of the applied control loops, the results of the Predictive/Analytical AVEVA simulation were compared against corresponding plant data. The percentage deviation was calculated using Equation (29) and is presented for all major process flows in Figure 19.

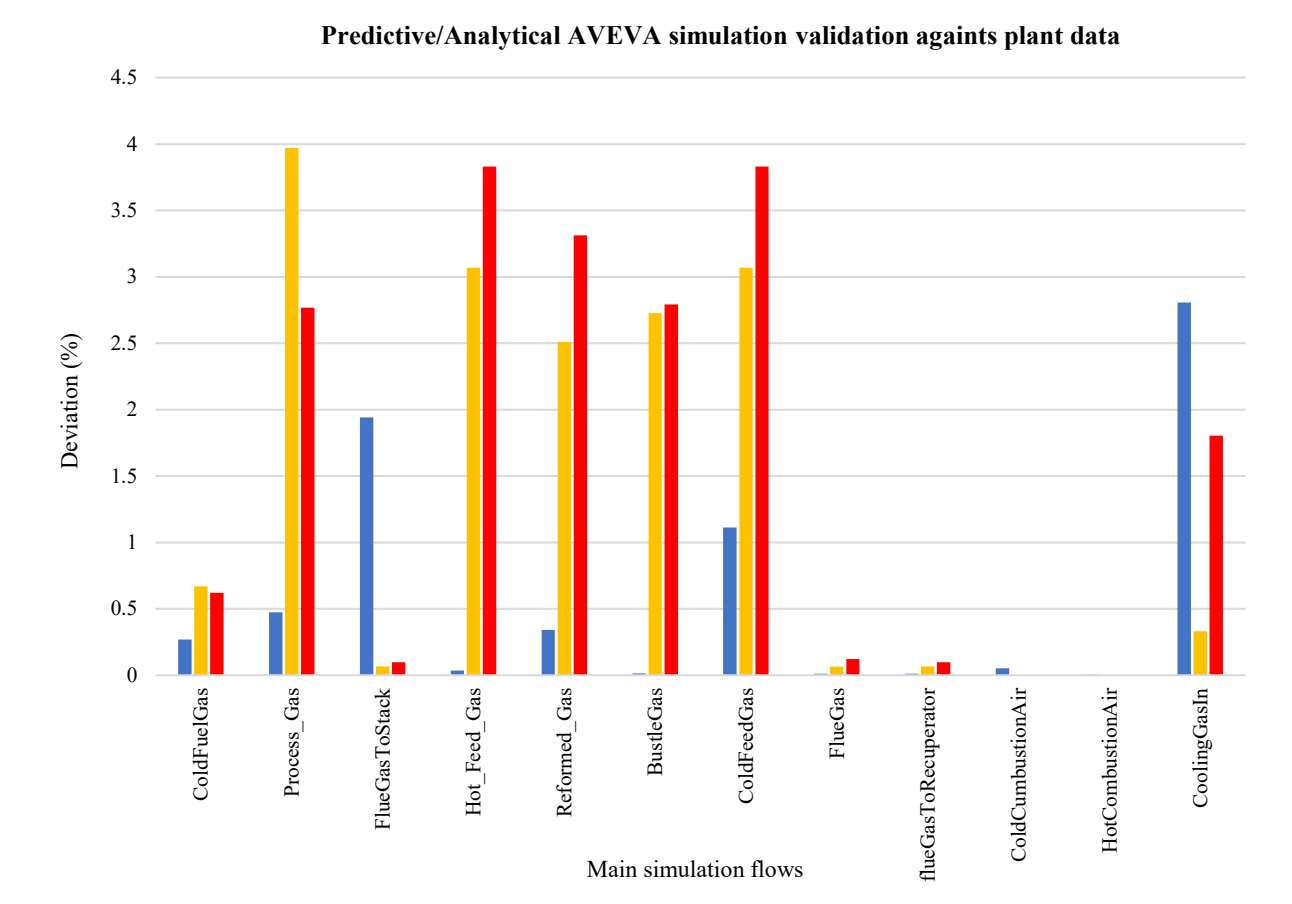


Figure 19. Deviation percentage of Predictive/Analytical AVEVA simulation validation against plant data

Although the deviations shown in Figure 19 are slightly higher than those observed in the fully constrained Analytical simulation (see Figure 18), all values remain within a 5% deviation threshold, which is generally accepted for industrial-scale simulation validation. This confirms the robustness and reliability of the Predictive/Analytical model. The slightly increased average deviation can be attributed to the additional degrees of freedom introduced in the Predictive/Analytical setup. These flexible boundaries, governed by the control loops, allow for broader variations in process conditions, which naturally introduces greater complexity and sensitivity compared to the fixed operating points used in the analytical model. Nevertheless, the deviation remains well within acceptable engineering margins, validating the suitability of the Predictive/Analytical simulation framework for further case studies and scenario analyses.

## 2. 3. DDRIVE – Dynamic DRI Virtual Environment

After having a validated Predictive/Analytical AVEVA simulation, the process simulation is ready to be integrated to the shaft furnace model in order to establish a comprehensive dynamic simulation of the DRI plant called DDRIVE (Dynamic DRI Virtual Environment). As previously discussed, the shaft furnace operates as a highly complex multi-zone reactor, where each zone is governed by distinct thermodynamic and kinetic phenomena. These zones facilitate a series of gas—solid reactions, which are summarized in Table 1.

#### 2. 3. 1. DDRIVE - Configuration

To overcome this limitation, a dedicated MATLAB model was developed in-house at ArcelorMittal. This advanced model is capable of simulating the spatially resolved temperature, flow, and composition fields inside the furnace, incorporating detailed reaction kinetics, mass and energy balances, and multi-phase flow interactions. It solves a set of coupled partial differential equations (PDEs) across a two-dimensional (2D) grid, capturing the radial and axial gradients in both solid and gas phases. The model includes:

- Multi-step reduction kinetics (Fe<sub>2</sub>O<sub>3</sub>  $\rightarrow$  Fe<sub>3</sub>O<sub>4</sub>  $\rightarrow$  FeO  $\rightarrow$  Fe) for both H<sub>2</sub> and CO-based reduction,
- Heat transfer mechanisms and momentum balances for both counter-current gas and downward-moving solid flow,
- Zone-specific gas injection and cooling behavior.

This 2D approach allows for a much finer resolution of the shaft furnace's internal behavior compared to conventional lumped-parameter models implemented in the literature so far. As a result, it can dynamically respond to changes in inlet gas composition, flow rates, and temperature coming from AVEVA simulation making it a powerful tool for predictive simulation and operational optimization. The temperature distribution at steady state operation of the 2D Shaft Furnace MATLAB model over the 3D geometry of plant with inlet and outlet flows are illustrated in Figure 20.

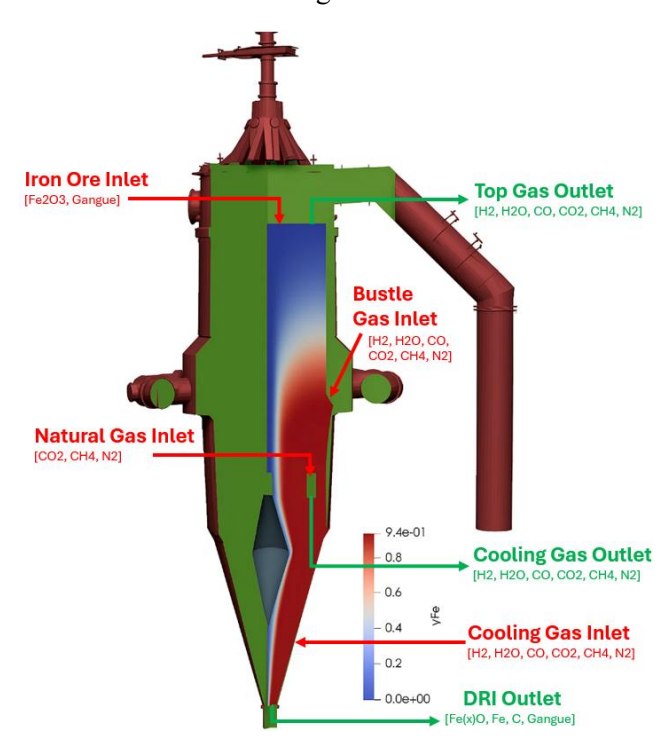


Figure 20. Temperature distribution in 2D Shaft Furnace MATLAB model over the 3D geometry of the shaft. Inlet and outlet flows are shown.

To connect the MATLAB 2D Shaft Furnace model to the AVEVA Predictive simulation a Python bridge code has been developed. Specifically, at each saving iteration, the output streams from the MATLAB shaft furnace simulation, Top Gas and Cooling Gas, are fed as input to the AVEVA model. Once the AVEVA simulation is solved, the resulting Bustle Gas and Cooling Gas streams are returned to the MATLAB shaft

model to update these parameters. The data flow enabling the dynamic robust simulation between MATLAB and AVEVA is presented at Figure 21.

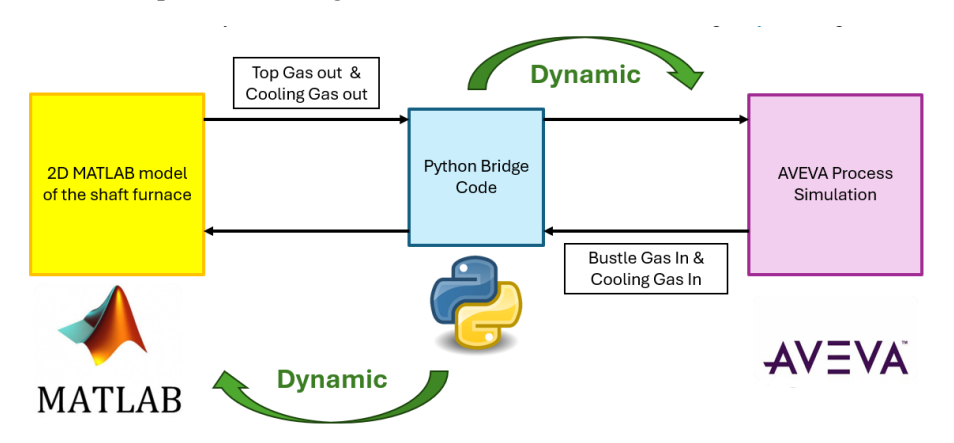


Figure 21. Diagram of dynamic flow of data between MATLAB and AVEVA stablishing DDRIVE model

#### 2. 3. 2. DDRIVE – Validation

To evaluate the correct accuracy of 2D MATLAB model of the shaft furnace and the reliability of its dynamic coupling with AVEVA Process Simulation, the deviation percentage (Equation (29)) and the absolute deviation (Equation (30)) of the Top Gas Outlet as one of the main results of the 2D MATLAB model of the shaft furnace and flows exchanged between MATLAB and AVEVA has been investigated in Figure 22 and Figure 23.

Absolte Deviation (%) = 
$$|Plant \, data - Simulation \, data|$$
 (30)

# **Top Gas Outlet Flow Properties Deviation**

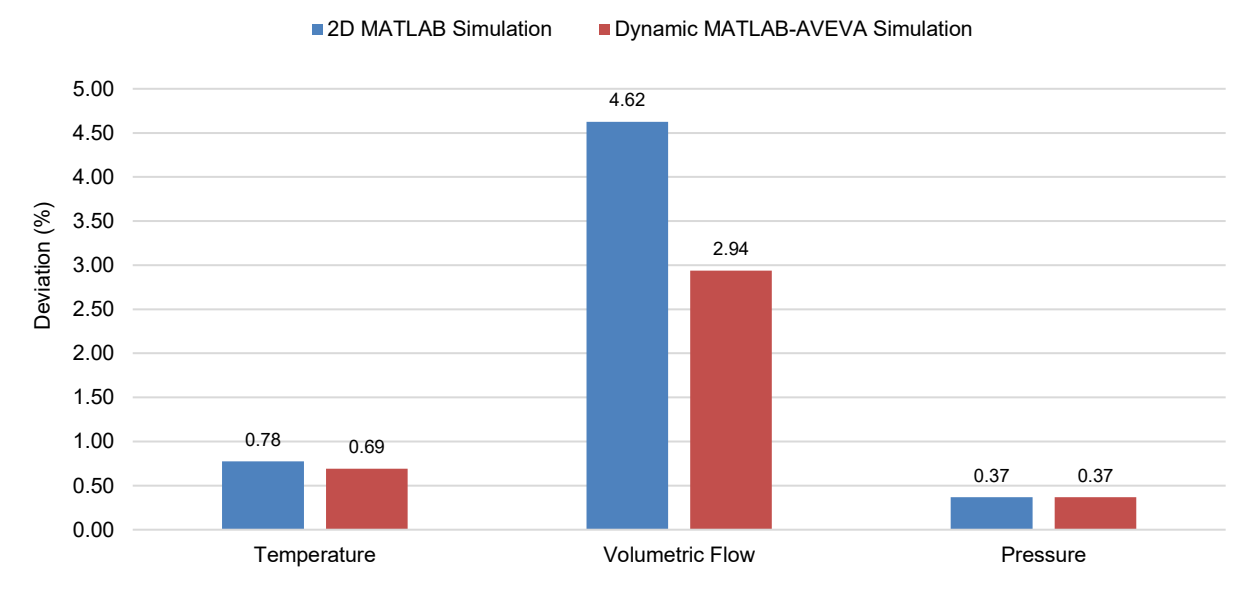


Figure 22. Top Gas Outlet flow properties deviation of 2D MATLAB shaft furnace simulation and DDRIVE compared to mass/energy balance data of the plant

22 - Advanced Dynamic Physical Simulation of Direct Iron Reduction Process in a Steel Plant

#### **Top Gas Outlet Composition Deviation**

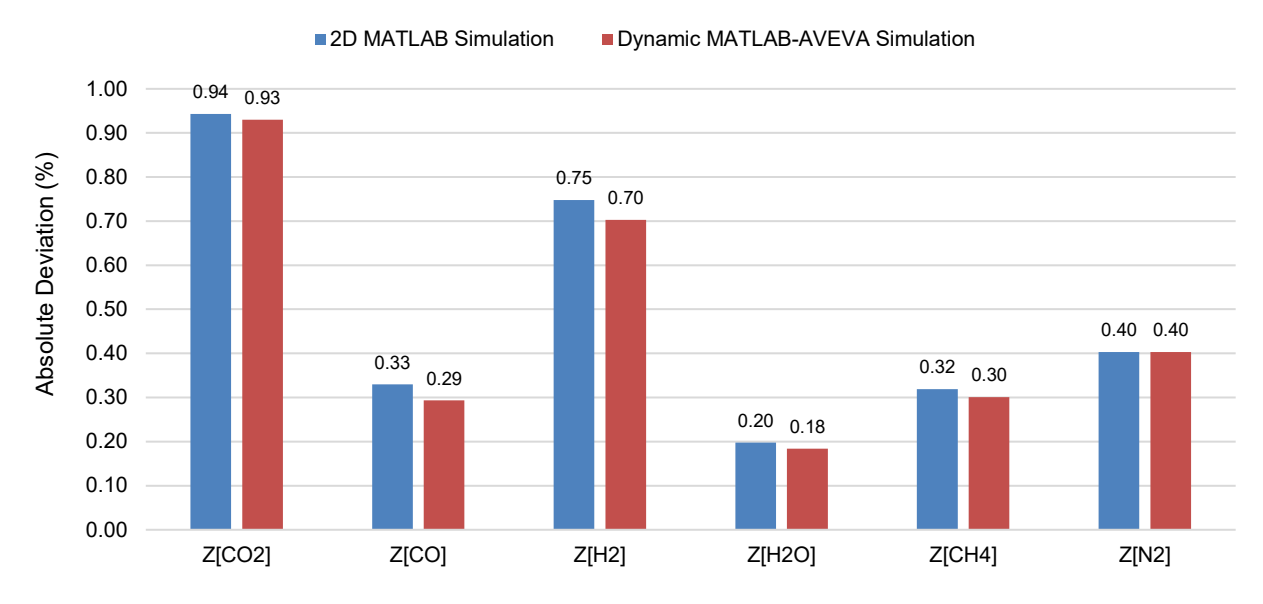


Figure 23. Top Gas Outlet flow composition deviation of 2D MATLAB shaft furnace simulation and DDRIVE compared to mass/energy balance data of the plant

As shown by the blue bars in Figure 22 and Figure 23, the 2D MATLAB shaft furnace simulation demonstrates strong agreement with reference data, with all deviations in the Top Gas Out properties and composition remaining below 5%. When integrated with AVEVA to form the DRRIVE, not only all deviations remain below 5%, but the deviations in all properties and most composition variables are further reduced. This outcome indicates that the DRRIVE not only provides detailed insights into the syngas production process, but also enhances the accuracy of the shaft furnace model by supplying dynamically updated and more realistic input data to the 2D MATLAB simulation.

## 3. Results and Case Studies

As discussed in pervious sections, the three simulation configurations, Analytical AVEVA Simulation, Predictive/Analytical AVEVA Simulation and Dynamic-Predictive Simulation, were validated against real plant data. This chapter presents and discusses the results of the dynamic behavior of the DRI process simulation under various operating conditions.

The first case study investigates the plant's dynamic response under its default operating mode, producing approximately 60 t/h of DRI, starting from a cold start-up and progressing to steady-state operation. The simulated plant, based on the ArcelorMittal DRI facility in Contrecoeur, Canada, is equipped to receive additional H<sub>2</sub> injection into the process gas. In the actual plant, seven distinct H<sub>2</sub> injection flow rates have been tested; these operating scenarios were replicated in the simulation, and the results were compared against plant measurements. In addition to assessing the agreement with measured data, the study examines the effect of H<sub>2</sub> injection on the key performance indicator of specific natural gas consumption. These analyses aim to evaluate the potential benefits of H<sub>2</sub> injection for performance optimization and decarbonization in DRI plants.

#### 3. 1. Default Plant Operation

This section presents the results of the plant's dynamic response under its default operating mode, corresponding to a production rate of approximately 60 t/h of DRI. In industrial practice, DRI plants undergo a preheating phase during start-up prior to reaching steady-state production. However, in this simulation, the analysis begins from a cold start-up condition, monitoring the process evolution until steady-state operation is achieved. These results provide a baseline for comparison with subsequent case studies involving process modifications, such as hydrogen injection.

Figure 24 illustrates the mass flow rate, metallization percentage, and composition of the solid DRI outlet in 24 hour of plant production form a cold start-up.

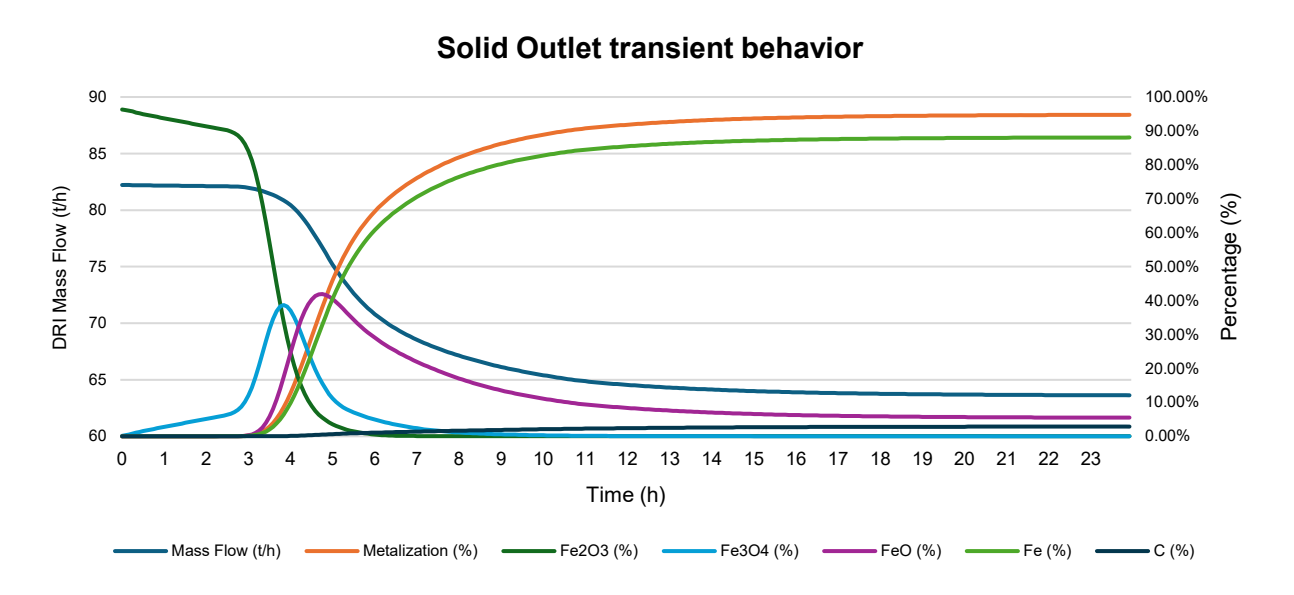


Figure 24. Dynamic behavior of the solid outlet in 24 hours of plant production from a cold start-up

As shown in Figure 24, the output mass flow rate of solid DRI initially matches the input flow rate of unrefined iron ore to the top of the shaft furnace, at 82 t/h, since no significant reduction has yet occurred. As the reduction reactions progress, the output mass flow rate decreases and eventually stabilizes at a steady DRI production rate of 63 t/h, corresponding to approximately 3% deviation from the plant data. At the outlet, a high-quality DRI is assured thanks to the final metalization rate of 94.75%. Figure 24 also clearly illustrates the sequential progression of the reduction reactions. Initially, around 87% of the iron ore in the solid DRI outlet consists of hematite (Fe<sub>2</sub>O<sub>3</sub>). As the proportion of hematite decreases, the proportion of magnetite (Fe<sub>3</sub>O<sub>4</sub>) increases, indicating the first stage of reduction, in which hematite is reduced to magnetite. Shortly thereafter, magnetite is further reduced to wüstite (FeO). In the final stage, wüstite is reduced to metallic iron (Fe), completing the sequence of reactions leading to the formation of DRI at the outlet.

The evolution of the top gas mole fraction of different species is presented in Figure 25.

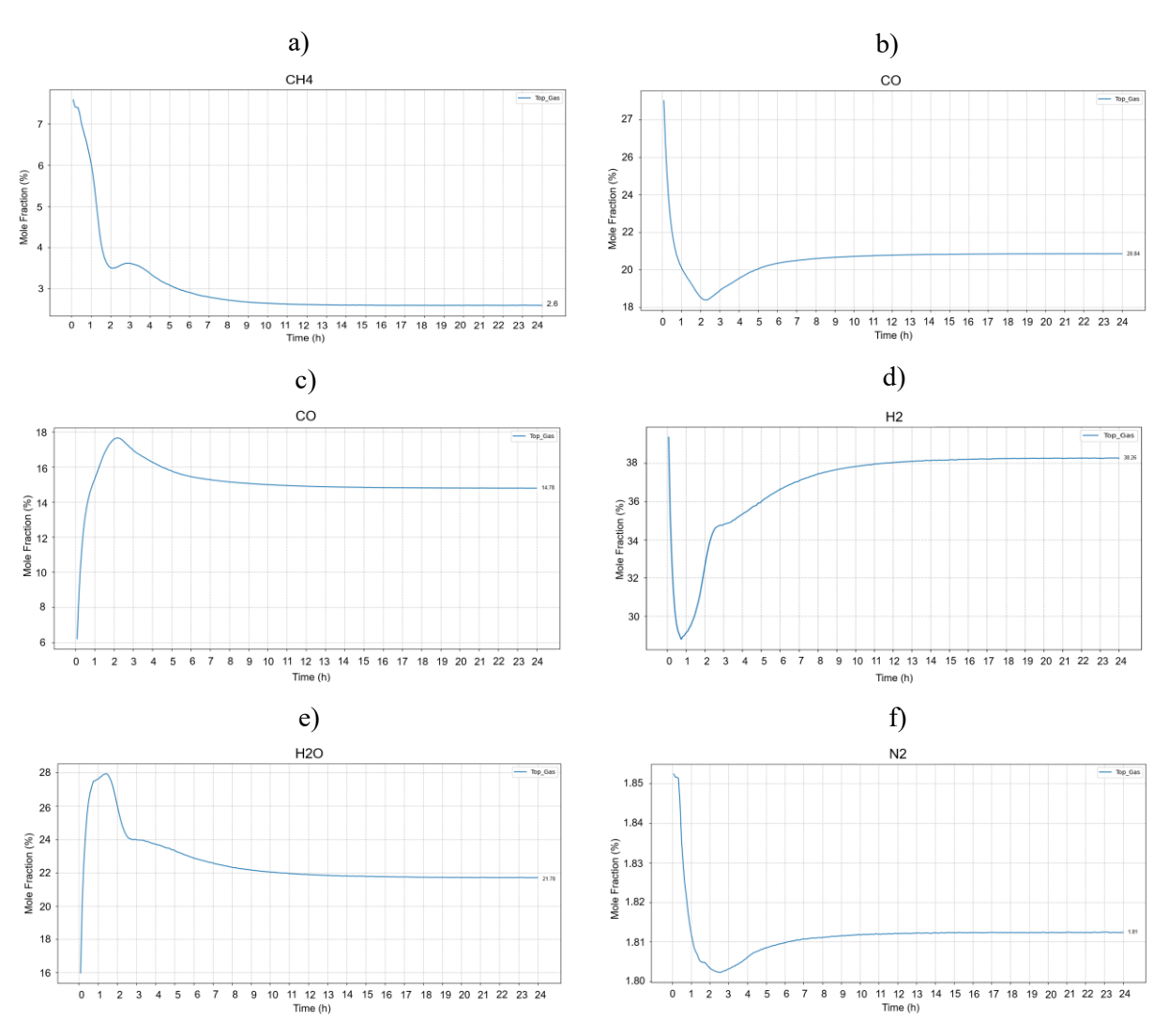


Figure 25. Mole fraction evolution of different species in the top gas during the 24-hour operation of the DRI plant from a cold start-up. a) CH<sub>4</sub>, b) CO<sub>2</sub>, d) H<sub>2</sub>, e) H<sub>2</sub>O, f) N<sub>2</sub>

Figure 25 illustrates the dynamic evolution of the top gas composition during the cold start-up of the shaft furnace until steady-state operation is achieved. The CH<sub>4</sub> mole fraction (Figure 25 - a) exhibits a sharp decline from approximately 7.2% to 3.7% within the first three hours, followed by a gradual decrease toward its steady-state value of 2.6%. The CO profile (Figure 25 - b) initially decreases from 28.5% to 18.4% due to incomplete reduction reactions, then progressively increases as the reforming reactions intensify, stabilizing at 20.8%. In contrast, CO<sub>2</sub> (Figure 25 - c) experiences a rapid rise from 6.4% to 17.7% during the early reduction phase, subsequently declining to its steady-state value of 14.8% as the reduction of iron oxides proceeds. The H<sub>2</sub> mole fraction (Figure 25 - d) initially drops from 39.2% to 28.8% due to rapid consumption in the early reduction reactions, then increases steadily to 38.3% as reforming reactions replenish hydrogen levels. Similarly, H<sub>2</sub>O (Figure 25 - e) increases sharply in the initial phase to about 20.1%, reflecting water formation from reduction reactions, and then decreases to 21.7% as the balance between generation and removal is established. N<sub>2</sub> (Figure 25 - f) remains relatively stable throughout the process, showing only minor fluctuations between 1.0% and 1.85%, indicative of its inert behavior in the

system. These compositional trends collectively demonstrate the interplay between reforming, reduction, and gas recirculation in determining the dynamic characteristics of the top gas.

# 3. 2. H<sub>2</sub> Injection Case Studies

After analyzing the default operation of the DRI plant during 24 hour from a cold start-up as a base line, cases with extra hydrogen injection that were already tested in the plant were simulated to investigate the effect of H<sub>2</sub> injection on key performance indicators, including CO<sub>2</sub> emissions, natural gas (NG) consumption, overall energy consumption, and bustle gas quality. The injection stage in the DRI syngas production is shown in Figure 26.

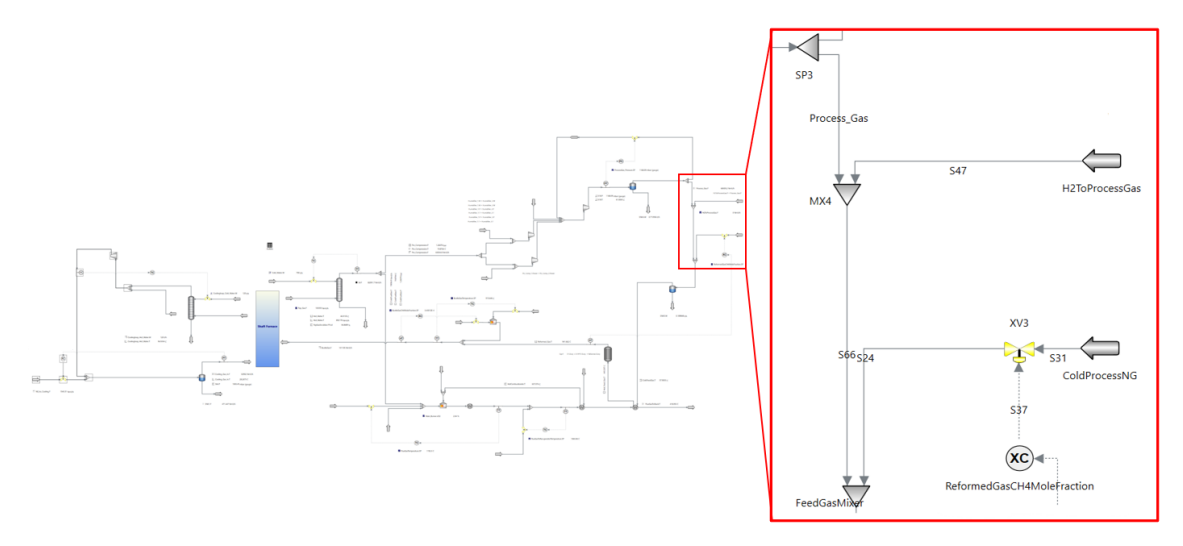


Figure 26. Schematic of H2 injection into the process gas before cold process natural gas injection in the DRI plant

Hydrogen injection experiments were conducted at seven different volumetric flow rates: 2600, 3215, 3317, 3412, 3949, 4128, and 4760 Nm<sup>3</sup>/h. Each injection level was maintained for a duration of three hours, as illustrated in Figure 27.

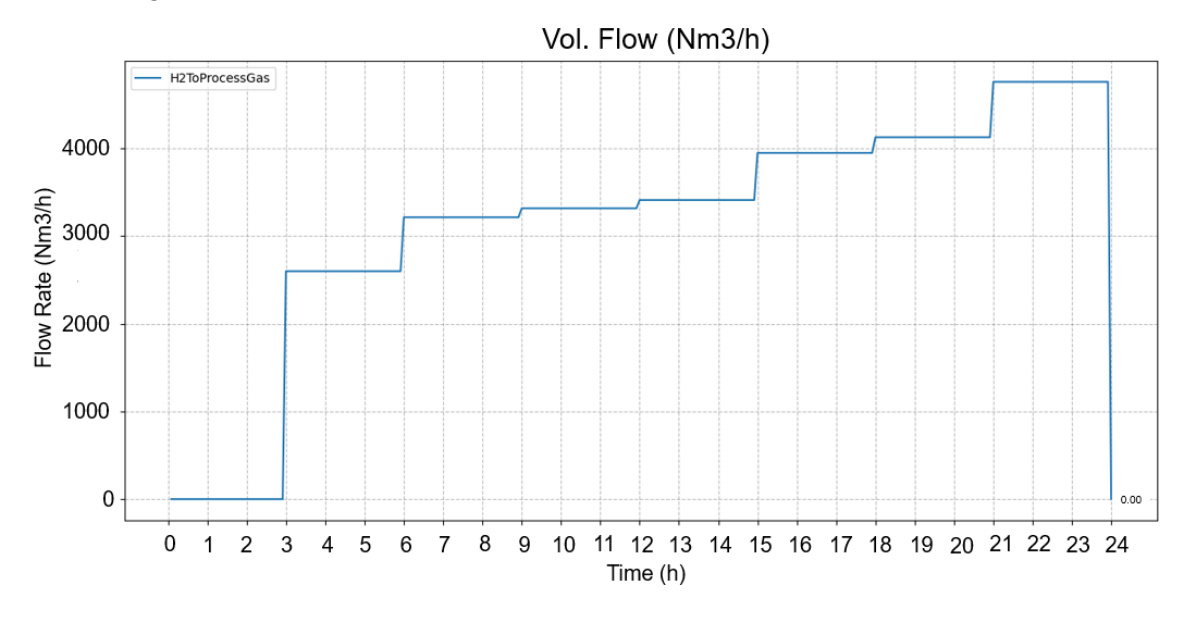


Figure 27. H<sub>2</sub> volumetric flow rate injection pattern

26 - Advanced Dynamic Physical Simulation of Direct Iron Reduction Process in a Steel Plant

The influence of varying hydrogen injection rates on the molar composition of the reformed gas is presented in **Error! Reference source not found.**.

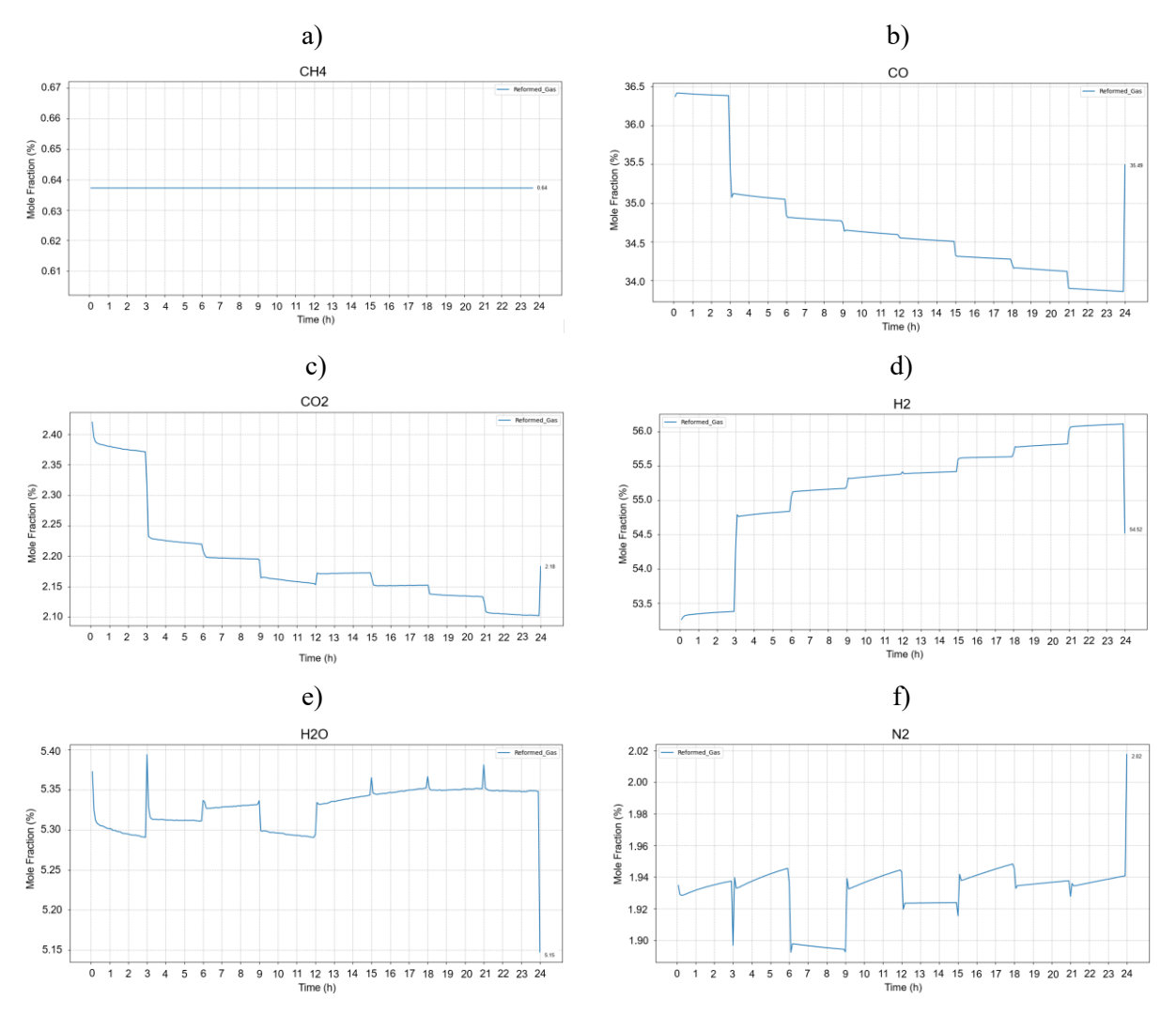


Figure 28. Reformed Gas molar fraction composition at different levels of H2 injections a)  $CH_4$ , b) CO, c)  $CO_2$ , d)  $H_2$ , e)  $H_2O$ , f)  $N_2$ 

The compositional profiles in Error! Reference source not found. indicate that hydrogen enrichment in the reformed gas increases proportionally with the injected H<sub>2</sub> flow rate (Figure 28 – d), while CO content decreases accordingly (Figure 28 – b). This inverse relationship reflects the shift in the syngas composition driven by the partial replacement of natural gas with hydrogen, thereby altering the reforming reaction equilibrium. The CO<sub>2</sub> concentration (Figure 28 – c) exhibits minor fluctuations, primarily due to the coupled effects of the water-gas shift reaction and variations in the overall syngas production rate. Meanwhile, the molar fractions of H<sub>2</sub>O and N<sub>2</sub> (Figure 28 – e, f) show moderate sensitivity to the hydrogen injection rate, with changes arising from both combustion stoichiometry adjustments and dilution effects. The CH<sub>4</sub> content (Figure 28 – a) remains constant across all tested scenarios, as it is actively controlled through the Cold NG to Process control loop to ensure the target quality of the Reformed Gas, and consequently, the quality of the Bustle Gas. These results highlight the capacity of hydrogen injection to significantly modify the reducing gas composition, which in turn can influence reduction kinetics in the shaft furnace. The observed

trends underscore the importance of precise control strategies to balance the competing objectives of maintaining optimal bustle gas quality while achieving the desired decarbonization targets.

To evaluate the decarbonization potentials, specific NG consumption at each flow rate of extra H<sub>2</sub> injection in the DRI process is compared in Figure 29.

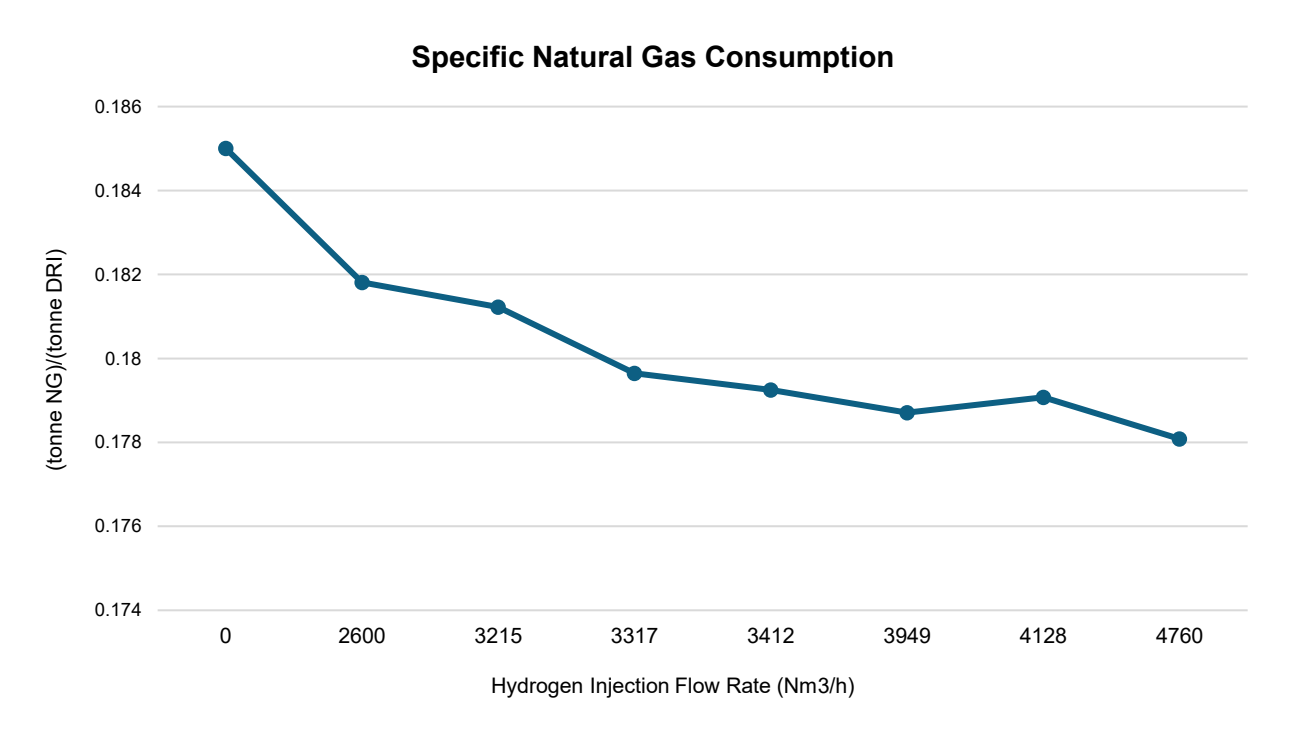


Figure 29. Specific natural gas consumption at different hydrogen injection flow rates

The baseline case without hydrogen injection corresponds to the highest specific NG consumption. As hydrogen injection is progressively introduced, a clear downward trend is observed, indicating that substituting part of the reducing gas with hydrogen reduces the overall NG demand of the process. Between 0 and 2600 Nm³/h of hydrogen injection, the reduction in specific NG consumption is particularly pronounced, dropping by nearly 2%. Beyond this threshold, the reduction continues but at a more gradual rate. At the maximum H<sub>2</sub> injection rate studied, 4760 Nm³/h, the specific NG consumption is reduced by approximately 3.9%. This trend highlights a key operational advantage. Hydrogen acts as a highly efficient reducing agent that bypasses the endothermic reforming reaction required by methane, leading to direct and immediate energy savings.

After analysing the reduction in fossil fuel consumption by replacing it with hydrogen, the specific CO<sub>2</sub> emission is illustrated in Figure 30, expressed as (tonne<sub>CO2</sub>/tonne<sub>DRI</sub>), for different hydrogen injection rates.

# 0.466 0.465 0.464 0.463 0.462 0.461 0.469 0.459 0.458

Figure 30. Specific CO<sub>2</sub> emission at different hydrogen injection flow rates

Hydrogen Injection Flow Rate (Nm3/h)

3317

3412

4128

3949

4760

0.457

2600

3215

The baseline case without hydrogen injection exhibits a specific emission of approximately 0.465 tonne<sub>CO2</sub> /tonne<sub>DRI</sub>. As hydrogen is introduced into the process gas, a clear downward trend in CO<sub>2</sub> emissions is observed, with the value decreasing to 0.459 tonne<sub>CO2</sub>/tonne<sub>DRI</sub> at the highest injection rate of 4760 Nm<sup>3</sup>/h. This corresponds to a reduction of about 1.3% relative to the baseline case. This trend is consistent with the results of Figure 29, where the specific natural gas consumption decreased steadily with increasing hydrogen injection. Together, the two results demonstrate the dual advantage of hydrogen injection. It simultaneously reduces the reliance on natural gas, a fossil fuel with a high carbon footprint, and decreases the specific CO<sub>2</sub> emissions of the plant. Even though the relative reduction in CO<sub>2</sub> intensity may appear modest, it is important to recognize that these results were obtained for very small hydrogen injection rates. Extrapolating this trend to higher substitution levels suggests a significant potential for further emission reductions, supporting the role of hydrogen as a key enabler for deep decarbonization of the direct reduction process. Qualitatively, the results highlight how shifting the reducing agent balance away from CO toward H<sub>2</sub> modifies the gas-solid reaction environment inside the shaft furnace. The increased share of H<sub>2</sub> reduction leads to greater H<sub>2</sub>O production in the top gas and, correspondingly, less CO<sub>2</sub> generation. Quantitatively, the reduction of approximately 6 kg CO<sub>2</sub> saved per tonne of DRI achieved at the highest tested injection rate, at the industrial scale of this plant with a production rate of 63.5 t<sub>DRI</sub>/h, translates into approximately 3600 tonnes of CO<sub>2</sub> annual reduction.

In conclusion, these findings validate the benefits of hydrogen injection as a decarbonization strategy for DRI plants. While the current study is limited to moderate substitution levels, the downward trend in both specific natural gas consumption and CO<sub>2</sub> emissions strongly supports further investigation of higher hydrogen injection rates as an effective pathway toward low-carbon ironmaking.

While the environmental and operational benefits of hydrogen injection are evident from the reductions in both specific CO<sub>2</sub> emissions and natural gas consumption, its economic viability ultimately determines the feasibility of large-scale industrial implementation. To assess this aspect, reference is made to the study "Hydrogen and the Decarbonization of Steel Production in Canada", performed by Adnan Khan et al. [42], which reports hydrogen and natural gas prices under several possible Canadian market conditions. Using this report, four scenarios are studied, reflecting different production pathways and infrastructure assumptions:

Scenario 1: Delivery of blue hydrogen to the Hamilton region (home to ArcelorMittal Dofasco) from nearby U.S. states such as Michigan, Ohio, or Pennsylvania, which offer suitable geology for carbon capture and sequestration (CCS). Hydrogen would be transported via a dedicated 400 km pipeline. Under this scenario, the delivered cost of blue hydrogen is estimated at C\$3.1/kg H<sub>2</sub>, assuming a natural gas price of C\$4/GJ from the point of hydrogen production.

Scenario 2: Similar to Scenario 1, but with the steel industry acting as an anchor tenant for infrastructure development serving multiple sectors (e.g., heavy transport, agriculture, space heating). By expanding throughput in the 400 km pipeline to supply a broader demand base, the delivered cost of blue hydrogen decreases to approximately C\$2.50/kg H<sub>2</sub>.

Scenario 3: Producing green hydrogen in Canada with low-carbon electricity delivered at C\$126/MWh. In this case, the cost of hydrogen would be about \$7.46/kg H<sub>2</sub> (C\$53/GJ H<sub>2</sub>). The price for natural gas is considered C\$5.5/GJ for the NG price of the steel industry.

Scenario 4: Using low-GHG electricity from future large-scale wind and solar deployment of C\$30/MWh to make green hydrogen. The resulting price would be C\$3.46/kg H<sub>2</sub> (C\$24/GJ). The price for natural gas is considered C\$5.5/GJ for the NG price of the steel industry.

Based on these four scenarios, the Specific Fuel Cost (SFC) in Canadian dollars per tonne of DRI was calculated, incorporating the combined cost of natural gas and hydrogen. The results are presented in Figure 31, illustrating the economic implications of different hydrogen supply pathways for DRI production.

#### Specific Fuel Cost

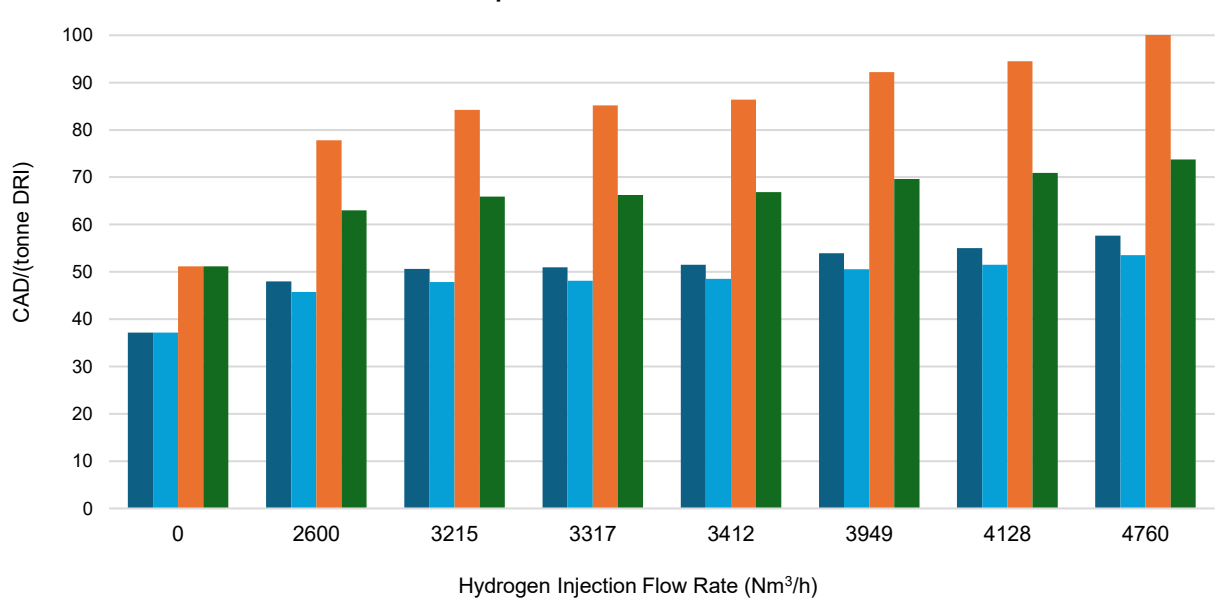


Figure 31. Specific Fuel Cost at different hydrogen injection flow rates

At the baseline condition without hydrogen injection, the SFC is tied exclusively to the natural gas price. Under these circumstances, the specific fuel cost is approximately 37 CAD/t DRI for Scenarios 1 and 2 (blue hydrogen assumptions) and 51 CAD/t DRI for Scenarios 3 and 4 (green hydrogen assumptions). These baseline values reflect the sole contribution of natural gas, priced at C\$4/GJ in the blue hydrogen scenarios and C\$5.5/GJ in the green hydrogen scenarios. This establishes the economic reference point for evaluating the effect of hydrogen substitution. H<sub>2</sub>

As hydrogen injection increases, the SFC trajectories diverge significantly across the four scenarios. For all injection rates, the highest SFC is observed in Scenario 3, corresponding to green hydrogen produced from current low-carbon electricity. With hydrogen costs reaching C\$7.46/kg H<sub>2</sub>, this scenario leads to SFC values exceeding 90–100 CAD/t DRI at high injection rates, making it the least competitive pathway in the near term. This result highlights a critical barrier to green hydrogen deployment in the short to medium term: the prevailing cost of low-carbon electricity results in prohibitively high hydrogen prices that directly undermine the economic feasibility of large-scale hydrogen substitution in DRI plants. In contrast, Scenario 2 consistently offers the lowest SFC among the hydrogen injection cases. In this scenario, blue hydrogen is imported from nearby U.S. states with suitable geology for carbon capture and storage (CCS), and economies of scale are assumed through multi-sectoral demand sharing of a 400 km hydrogen pipeline. With delivered hydrogen costs of C\$2.50/kg H<sub>2</sub>, the SFC increases only moderately with higher injection rates. Quantitatively, under Scenario 2, the cost advantage remains tangible up to an injection level of approximately 3949 Nm<sup>3</sup>/h, beyond which the rising cost of hydrogen begins to offset the savings from reduced natural gas consumption. This finding suggests that blue hydrogen supply chains, when integrated with CCS and cross-sector infrastructure, offer the most realistic medium-term pathway to cost-effective decarbonization of DRI plants in regions such as Québec or Ontario. At Scenario 1, its SFC values lie consistently above those of Scenario 2, though still below those of green hydrogen scenarios at lower

injection rates. This highlights the importance of shared infrastructure and cross-sector collaboration for reducing hydrogen delivery costs.

Taken together, these results underscore a fundamental trade-off. Although hydrogen injection clearly reduces natural gas consumption and CO<sub>2</sub> emissions, its cost competitiveness depends critically on the price and supply pathway of hydrogen. Blue hydrogen with CCS and economies of scale (Scenario 2) emerges as the only near-term economically viable pathway, while current green hydrogen (Scenario 3) remains too costly. Future renewable-driven green hydrogen (Scenario 4) offers long-term promise, provided that electricity costs fall to projected levels. Thus, while environmental analysis supports hydrogen injection as a key lever for decarbonization, the economic analysis clearly emphasizes the decisive role of hydrogen pricing and infrastructure development. Policy support for CCS deployment, hydrogen pipelines, and renewable expansion will therefore be central to determining whether hydrogen-based DRI can achieve large-scale viability

#### 3. 3. Future Work

The dynamic simulation framework developed in this thesis provides a powerful foundation for the analysis of direct reduced iron (DRI) plants. By enabling a detailed representation of both the shaft furnace and the surrounding syngas loop, the model allows the plant's behavior to be studied without the need for extensive experimental campaigns. Building on this foundation, several directions for future research can be identified.

First, the current study has focused on moderate hydrogen injection rates. Future investigations should extend this analysis to higher hydrogen enrichment levels in order to systematically explore the opportunities and operational challenges associated with deeper decarbonization. Such studies would allow the identification of thresholds beyond which process stability, metallization, or energy efficiency may be compromised. Second, the Python bridge code developed to link AVEVA and MATLAB offers significant potential for further development. Since this interface is capable of controlling and analyzing the AVEVA environment dynamically, it provides a natural platform for integrating advanced optimization methods, including machine learning and artificial intelligence algorithms. These approaches could be employed to optimize burner firing, purge strategies, reformer operation, or hydrogen injection schedules, thereby improving both energy efficiency and emission performance. Finally, the comprehensive dataset generated by the DDRIVE framework, covering every stream and reaction step in the process, can serve as the basis for comprehensive carbon mass balance validation and extended techno-economic analyses. For example, exploring the economic viability of hydrogen injection under a broader set of price scenarios and injection rates to find optimized viable points of green DRI production. This would provide valuable insights into the trade-offs between decarbonization potential and economic competitiveness, supporting industry-wide decision-making in the transition to low-carbon steel production. Coupling the DDRIVE framework with life-cycle assessment (LCA) tools to quantify indirect emissions and upstream fuel costs presents another opportunity for researchers.

#### 4. Conclusion

The iron and steel industry faces increasing pressure to decarbonize, with direct reduced iron (DRI) processes recognized as one of the most promising alternatives to conventional blast furnace—basic oxygen furnace (BF–BOF) routes. However, the inherent complexity of the DRI process, which involves multiple recycle loops, endothermic reforming reactions, and the highly non-linear behavior of the shaft furnace, has limited the ability of conventional steady-state simulations to capture its full dynamic behavior.

The present work developed and validated a novel integrated dynamic simulation framework of a MIDREX-type DRI plant. The plant was modeled in two interconnected sections: (i) the syngas generation and gas recycling loop, constructed in AVEVA Process Simulation, and (ii) a two-dimensional MATLAB model of the shaft furnace, developed in-house by ArcelorMittal, representing the multi-zone reduction of iron ore pellets. These two environments were coupled through a Python bridge code, which enabled the iterative exchange of critical flow parameters. This integrated platform, referred to as the Dynamic DRI Virtual Environment (DDRIVE), represents the first attempt to capture the dynamic behavior of an entire DRI plant at this level of detail. The framework was validated against operational data from ArcelorMittal's Contrecœur DRI plant. Across all major process variables, including gas composition, temperature, and flow rate, the deviations between model predictions and plant measurements remained within 5%, thereby confirming the robustness and reliability of the model. This validation provides confidence that the DDRIVE platform can be used not only for process analysis but also for scenario evaluation and predictive optimization.

Moreover, case studies were conducted to investigate both default plant operation and the effect of hydrogen injection into the process gas, which can be summarized as:

- Default operation shows a steady DRI production of ~63 t/h reached from a cold start, initial outflow 82 t/h equal to ore feed, with ~3 percent deviation relative to plant data.
- The final metalization rate of 94.75% assures high-quality DRI at the outlet.
- Hydrogen-injection test was performed at seven steps from 2600 to 4760 Nm<sup>3</sup>/h reproducing plant results.
- Specific NG consumption reduced by nearly 2% and 3.9% percent when extra hydrogen injection was raised from 0 to 2600 Nm<sup>3</sup>/h and 4760 Nm<sup>3</sup>/h.
- Hydrogen injection led to a clear downward trend in specific CO<sub>2</sub> emissions per tonne of DRI, demonstrating the potential of hydrogen to gradually decarbonize the process. Around 3600 tonnes of carbon dioxide emissions can be prevented per year with the hydrogen injection rate of 4760 Nm3/h.
- The SFC analysis revealed that while absolute costs depend heavily on hydrogen price scenarios, the general trend shows a trade-off between environmental benefits and economic feasibility. Current green hydrogen costs are not yet competitive, but blue hydrogen with CCS could make partial substitution both technically and economically viable in the near term, highlighting the importance of fuel cost trajectories in enabling large-scale adoption.

Beyond the findings of the present work, the developed DDRIVE framework also opens several promising avenues for future research. Higher levels of hydrogen enrichment should be systematically explored to assess both the decarbonization potential and the operational limitations of hydrogen-based DRI.

Furthermore, the Python–AVEVA interface offers a flexible platform for incorporating advanced optimization tools, including machine learning and artificial intelligence, to enhance process control and efficiency. Finally, the comprehensive process data generated by the model provides an opportunity for integrated techno-economic and environmental analyses, which will be essential for evaluating the large-scale industrial feasibility of hydrogen in direct reduction.

# 5. Bibliography

- [1] "CO<sub>2</sub> Emissions from Fuel Combustion," International Energy Agency (IEA)., 2020. [Online]. Available: https://www.iea.org/data-and-statistics. [Accessed 5 3 2025].
- [2] (IEA), International Energy Agency, "Iron and Steel Technology Roadmap," Paris, 2020.
- [3] Statistica, "World crude steel production from 2012 to 2023," World Steel Association, 9 10 2024. [Online]. Available: https://www.statista.com/statistics/267264/world-crude-steel-production/. [Accessed 10 3 2025].
- [4] I. P. o. C. C. (IPCC), "Climate Change 2022: Mitigation of Climate Change," 2022.
- [5] Ariyan Zare Ghadi, Mohammad Sadegh Valipour, Seyed Masoud Vahedi, Hong Yong Sohn, "A Review on the Modeling of Gaseous Reduction of Iron Oxide Pellets," *steel research int.*, vol. 91, no. 1, p. 1900270, 2019.
- [6] "Making Net-Zero Steel Possible: A Policy Framework for Decarbonising Steel," Energy Transitions Commission (ETC), London, UK, Oct. 2021.
- [7] B. B. Çiftçi, "Raw materials," worldsteel.org, [Online]. Available: https://worldsteel.org/othertopics/raw-materials/. [Accessed 10 3 2025].
- [8] Zhaoyang Li, Zheng Qi, Lechen Zhang, Meng Guo, Dong Liang, and Qiang Dong, "Numerical simulation of H2-intensive shaft furnace direct reduction process," *Journal of Cleaner Production*, vol. 409, p. 137059–137059, 2023.
- [9] Junhao Ling, Haitao Yang, Guocai Tian, Jiaxin Cheng, Xin Wang, Xiaohua Yu, "Direct reduction of iron to facilitate net zero emissions in the steel industry: A review of research progress at different scales," *Journal of Cleaner Production*, vol. 441, no. 140933, 2024.
- [10] Guanyong Sun, Bin Li, Hanjie Guo, Wensheng Yang, Shaoying L, Jing Guo, "Thermodynamic Study on Reduction of Iron Oxides by H2 + CO + CH4 + N2 Mixture at 900 °C," *Energies*, vol. 13 (19), no. 5053, 23 7 2020.
- [11] ". R. C. f. U. 2. P. Sikstrom, "Direct Reduction Concept for ULCOS a brief introduction," 2013.
- [12] Antonio Trinca, Daniele Patrizi, Nicola Verdone, Claudia Bassano, Giorgio Vilardi, "Toward green steel: Modeling and environmental economic analysis of iron direct reduction with different reducing gases," *Journal of Cleaner Production*, vol. 427, no. 139081, 15 November 2023.
- [13] Masaaki ATSUSHI, Hiroshi UEMURA, Takashi SAKAGUCHI, "Midrex Processes Kobelco," Kobelco, 2010.
- 35 Advanced Dynamic Physical Simulation of Direct Iron Reduction Process in a Steel Plant

- [14] Yan Ma, Isnaldi R. Souza Filho, Yang Bai, Johannes Schenk, Fabrice Patisson, Arik Beck, Jeroen A. van Bokhoven, Marc G. Willinger, Kejiang Li, Degang Xie, Dirk Ponge, Stefan Zaefferer, Baptiste Gault, Jaber R. Mianroodi, Dierk Raabe, "Hierarchical nature of hydrogen-based direct reduction of iron oxides," *Scripta Materialia*, vol. 213, no. 114571, 2022.
- [15] Hamzeh Hamadeh, Olivier Mirgaux, Fabrice Patisson, "Detailed Modeling of the Direct Reduction of Iron Ore in a Shaft Furnace," *Materials*, vol. 11(10):1865, 2018.
- [16] Basak Anameric, S. Komar Kawatra, "PROPERTIES AND FEATURES OF DIRECT REDUCED IRON," *Mineral Processing and Extractive Metallurgy Review*, vol. 28, no. 1, 2007.
- [17] Amaia Sasiain Conde, Katharina Rechberger, Andreas Spanlang, Hermann Wolfmeir, Christopher Harris, "Decarbonization of the steel industry. A techno-economic analysis.," *Matériaux & Techniques*, vol. 109, 2021.
- [18] Duncan Kushnir, Teis Hansen, Valentin Vogl, Max Åhman, "Adopting hydrogen direct reduction for the Swedish steel industry: A technological innovation system (TIS) study," *Journal of Cleaner Production*, vol. 242, no. 118185, 2020.
- [19] Wenguo Liu, Haibin Zuo, Jingsong Wang, Qingguo Xue, Binglang Ren, Fan Yang, "The production and application of hydrogen in steel industry," *International Journal of Hydrogen Energy*, vol. 46, no. 17, pp. 10548-10569, 2021.
- [20] Robert Millner, Johannes Rothberger, Barbara Rammer, Christian Boehm, Wolfgang Sterrer, Hanspeter Ofner, Vincent Chevrier, "MIDREX H2 The Road to CO2-free Direct Reduction," in *Proc. AISTech 2021*, Nashville, 2021.
- [21] Niall Mac Dowell, Nixon Sunny, Nigel Brandon, Howard Herzog, Anthony Y. Ku, Wilfried Maas, Andrea Ramirez, David M. Reiner, Gaurav N. Sant, Nilay Shah,, "The hydrogen economy: A pragmatic path forward," *Joule*, vol. 5, no. 10, 2021.
- [22] Yan Ma, Isnaldi R. Souza Filho, Yang Bai, Johannes Schenk, Fabrice Patisson, Arik Beck, Jeroen A. van Bokhoven, Marc G. Willinger, Kejiang Li, Degang Xie, Dirk Ponge, Stefan Zaefferer, Baptiste Gault, Jaber R. Mianroodi, Dierk Raabe., "Hierarchical nature of hydrogen-based direct reduction of iron oxides," *Scripta Materialia*, vol. 213, no. 114571, 2022.
- [23] Zhao-cai Wang, Man-sheng Chu, Zheng-gen Liu, Zhuang-yin Chen & Xiang-xin Xue, "Effects of Temperature and Atmosphere on Pellets Reduction Swelling Index," *Journal of Iron and Steel Research International*, vol. 19, p. 7–12, 2012.
- [24] A. BONALDE, A. HENRIQUEZ, M. MANRIQUE, "Kinetic Analysis of the Iron Oxide Reduction Using Hydrogen-Carbon Monoxide Mixtures as Reducing Agent," *ISIJ International*, vol. 45, no. 9, pp. 1255-1260, 2005.

- [25] A. A. EI-GEASSY, K. A. SHEHATA, S. Y. EZZ, "Mechanism of Iron Oxide Reduction with Hydrogen/Carbon Monoxide Mixtures," *Transactions of the Iron and Steel Institute of Japan*, vol. 17, no. 11, pp. 629-635, 1977.
- [26] Lingyun Yi, Zhucheng Huang, Tao Jiang, Ronghai Zhong, Zhikai Liang, "Iron ore pellet disintegration mechanism in simulated shaft furnace conditions," *Powder Technology*, vol. 317, pp. 89-94, 2017.
- [27] Hai-bin Zuo, Cong Wang, Jie-ji Dong, Ke-xin Jiao & Run-sheng Xu, "Reduction kinetics of iron oxide pellets with H2 and CO mixtures," *International Journal of Minerals, Metallurgy, and Materials*, vol. 22, p. 688–696, 2015.
- [28] Daniel Spreitzer, Johannes Schenk, "Reduction of Iron Oxides with Hydrogen—A Review," *steel* research int., vol. 90, no. 10, 2019.
- [29] Run-sheng Xu, Jian-liang Zhang, Hai-bin Zuo, Ke-xin Jiao, Zheng-wen Hu & Xiang-dong Xing, "Mechanisms of swelling of iron ore oxidized pellets in high reduction potential atmosphere," *Journal of Iron and Steel Research International*, vol. 22, p. 1–8, 2015.
- [30] Patrícia Metolina, Tiago Ramos Ribeiro & Roberto Guardani, "Hydrogen-based direct reduction of industrial iron ore pellets: Statistically designed experiments and computational simulation," *International Journal of Minerals, Metallurgy and Materials*, vol. 29, p. 1908–1921, 2022.
- [31] Patrícia Metolina, Roberto Silva de Andrade, Bruno Ramos, Roberto Guardani, "Hydrogen direct reduction ironmaking process for zero CO2 emission: A study on the effect of particle properties changes during the multiple non-catalytic gas-solid reactions," *Minerals Engineering*, vol. 201, no. 108188, 2023.
- [32] N. Müller, G. Herz, E. Reichelt, "CO2 Emission Reduction Potential in the Steel Industry by Integration of a Direct Reduction Process into Existing Steel Mills," IAEA, Dresden, 2018.
- [33] Rami Béchara, Hamzeh Hamadeh, Olivier Mirgaux and Fabrice Patisson, "Carbon Impact Mitigation of the Iron Ore Direct Reduction Process through Computer-Aided Optimization and Design Changes," *Metals*, vol. 10, no. 3, p. 367, 2020.
- [34] Katharina Rechberger, Andreas Spanlang, Amaia Sasiain Conde, Hermann Wolfmeir, Christopher Harris, "Green Hydrogen-Based Direct Reduction for Low-Carbon Steelmaking," *steel research international*, vol. 91, no. 11, 2020.
- [35] Jake Immonen, Kody M. Powell, "Dynamic modeling of a direct reduced iron shaft furnace to enable pathways towards decarbonized steel production," *Chemical Engineering Science*, vol. 300, 2024.
- [36] S. M. Alsaedi, "Design and Analysis of Hydrogen Based Direct," *Master of Science thesis, Chemical Engineering Department, Khalifa University, Abu Dhabi,* 2023.
- 37 Advanced Dynamic Physical Simulation of Direct Iron Reduction Process in a Steel Plant

- [37] Jianguo Xu, Gilbert F. Froment, "Methane steam reforming, methanation and water-gas shift: I. Intrinsic kinetics," *AlChE Journal*, vol. 35, no. 1, pp. 88-96, January 1989.
- [38] Abdelhamid Ajbar, Khalid Alhumaizi, Mustafa Soliman, "Modeling and simulations of a reformer used in direct reduction of iron," *Korean Journal of Chemical Engineering*, vol. 28, no. 12, p. 2242–2249, February 2011.
- [39] Xiaowei Huang, Rainer Reimert, "Kinetics of steam reforming of ethane on Ni/YSZ (yttria-stabilised zirconia) catalyst," *Fuel*, vol. 106, pp. 380-387, 2013.
- [40] Johnny Saavedra Lopez, Vanessa Lebarbier Dagle, Chinmay A. Deshmane, Libor Kovarik, Robert S. Wegeng, Robert A. Dagle, "Methane and Ethane Steam Reforming over MgAl2O4-Supported Rh and Ir Catalysts: Catalytic Implications for Natural Gas Reforming Application," *Catalysts*, vol. 9, no. 10, p. 801, 2019.
- [41] José Valecillos, Sergio Iglesias-Vázquez, Leire Landa, Aingeru Remiro, Javier Bilbao, Ana G. Gayubo, "Insights into the Reaction Routes for H2 Formation in the Ethanol Steam Reforming on a Catalyst Derived from NiAl2O4 Spinel," *Energy & Fuels*, vol. 35, no. 21, pp. 17197-17211, 2021.
- [42] Khan, M.A., Powell, M., Tampier, M., Thorn, E. and Layzell, D., "Hydrogen and the Decarbonization of Steel Production in Canada: Reaching," vol. 5, no. 2, pp. 1-145, 2023.